Comprehensive Summaries of Uppsala Dissertations
from the Faculty of Science and Technology 923

All-Thin-Film Electrochromic Devices for Optical and Thermal Modulation

BY

ANNA-LENA LARSSON

ACTA UNIVERSITATIS UPSALIENSIS
UPPSALA 2004

Dissertation presented at Uppsala University to be publicly examined in Häggsalen, The Ångström Laboratory, Uppsala, Friday, January 30, 2004 at 09:00 for the degree of Doctor of Philosophy. The examination will be conducted in English.

Abstract

Larsson, A-L. 2004. All-Thin-Film Electrochromic Devices for Optical and Thermal Modulation. Acta Universitatis Upsaliensis. *Comprehensive Summaries of Uppsala Dissertations from the Faculty of Science and Technology* 923. 54 pp. Uppsala. ISBN 91-554-5844-0

The optical properties of electrochromic materials can be changed by application of an electrical voltage. The conventional electrochromic device consists of several thin films of electrochromic materials and layers for electron- and ion conduction. The ion conductor in devices intended for applications using visible light is often a polymer electrolyte that is used to laminate two half-cells together. The miniaturization of satellites has led to reduced mass and volume available for systems to handle temperature variations onboard. The satellite will be submitted to large variations in the radiating environment in an earth bound orbit. An electrochromic device could provide adaptable radiation exchange due to its variable infrared optical properties. The polymer electrolyte is not a desirable component in the space environment, but it can be replaced by an inorganic thin film so that an all-thin-film (ATF) device is obtained.

This thesis investigates the optical properties of amorphous and crystalline WO_3, as well as the performance of ATF devices with sputtered ZrO_2 as the ion conductor. The infrared reflectance for Li-intercalated WO_3 has been measured in the wavelength range 2-50 mm. The near infrared absorption for low intercalation levels showed good agreement with large polaron theory. The infrared reflectance increased with higher intercalation levels and exhibited a free-electron behaviour. The infrared reflectance of a laminated device with polymer electrolyte was measured, and the calculated emittance varied between 0.56 and 0.65. The ATF device consisted of thin films of WO_3, ZrO_2 and $NiV_xO_yH_z$, as well as evaporated Al top contacts. The substrates were commercial ITO on glass. The emittance for different device designs was calculated from reflectance measurements, and could be varied between 0.33 and 0.59. This makes them strong contenders to other contemporary emittance modulating devices.

Anna-Lena Larsson, Department of Engineering Sciences, Box 534, Uppsala University, SE-751 21 Uppsala, Sweden

ISSN 1104-232X
ISBN 91-554-5844-0
urn:nbn:se:uu:diva-3917 (http://urn.kb.se/resolve?urn=urn:nbn:se:uu:diva-3917)

Printed in Sweden by Universitetstryckeriet, Uppsala 2004

List of Papers

I Functional surfaces for thermal control
Larsson A.-L., Niklasson G.A. and Stenmark L.
Proc. 3rd Round Table on Micro/Nano-Technologies for Space, **WPP-174** (2000) 249.

II Infrared optical properties of sputtered WO_3
Larsson A.-L., Niklasson G.A. and Stenmark L.
Proc. SPIE, **4102** (2000) 69.

III H+ Conduction Parameters in Solid-State Electrochromic Devices Obtained by the Isothermal Transient Ionic Current Technique
Jonsson A.K., Larsson A.-L., Niklasson G.A. and Strømme, M..
J. Electrochem. Soc (submitted)

IV Optical absorption of Li-intercalated polycrystalline tungsten oxide films: Comparison to large polaron theory
Larsson A.L., Sernelius B.E. and Niklasson G.A.
Solid State Ion., **165** (2003) 35.

V Optical properties of electrochromic all-solid-state devices
Larsson A.L. and Niklasson G.A
Solar Energy Mater. Solar Cells (submitted)

VI Infrared absorption of Li-intercalated tungsten oxide
Larsson A.-L., Solis J. and Niklasson G.A.
Solar Energy Mater. Solar Cells (submitted)

VII Infrared emittance modulation of all-thin film electrochromic devices
Larsson A.-L. and Niklasson G.A.
Materials Lett. (submitted)

Comments on my contribution

I	Sample preparation, most of the measurements and writing
II,V, VII	Sample preparation, measurements, most of the writing
III	Sample preparation, part of the writing
IV	Sample preparation, measurements, part of the writing
VI	Sample preparation, measurements on amorphous and polycrystalline WO_3, most of the writing

Publications not included in the thesis

i Thin film coatings with variable emittance
Larsson A.-L., Niklasson G. and Stenmark L.
Proc.SPIE **3738** (1999) 486.

ii Theoretical investigation of ion conduction in three-layered ion-conductor systems: derivation of the isothermal transient ionic current and frequency-dependent impedance
Frenning G., Jonsson A.K., Larsson A.L. and Strømme, M..
J.Appl. Phys. **94** (2003) 1629.

iii Electrochromic tungsten oxide: The role of defects
Niklasson G.A., Berggren L. and Larsson A.-L.
Solar Energy Mater. Solar Cells (submitted)

Abbreviations and acronyms

α	absorptance
asd	as deposited
A	area
ATF	all-thin-film
a-WO_3	amorphous WO_3
$B_{T,\lambda}$	black body spectrum
cv	cyclic voltammogram
c-WO_3	crystalline WO_3
CVD	chemical vapour deposition
d	thickness
DC	direct current
ε	dielectric function
ε_v	permittivity in vacuum
e	emittance
e_0	elementary charge of one electron
EM	electromagnetic
F	form factor
FTIR	Fourier transform infrared spectroscopy
ga	galvanostatic ampereometry
IR	infrared
ITO	tin doped indium oxide
λ	wavelength
LEO	low earth orbit
LiTFSI	lithium bis(trifluoromethylsulfone)imide
M	Molar mass
MEMS	micro-electromechanical system
N_A	Avogadros constant
NIR	near infrared
PC	propylene carbonate
PMMA	polymerized methyl methacrylate

PVD	physical vapour deposition
q	heat flow
Q_{Li}	Li ion charge
r	reflectance coefficient
R	reflectance
RBS	Rutherford backscattering spectrometry
t	transmittance coefficient
T	transmittance
UV	ultraviolet
VIS	visible
ω	frequency
x	intercalated ion per atom
XRD	x-ray diffraction
ς	electron-phonon coupling factor
ÅSTC	Ångström space technology centre

Contents

1 Introduction

The temperature of a satellite must be controlled due to the requirements of payload and platform[ii]. This is of crucial importance for a successful mission. Cost is one of the large development drivers, and since launch cost is about proportional to mass[1] there is an increased activity in the development of miniaturized satellites. Many conventional thermal control systems have turned out to be too bulky or heavy for these small spacecraft, and functional surfaces are of great interest for the space industry. This thesis presents such a surface, an electrochromic device based on inorganic thin films, for modulation of radiation at infrared and optical wavelengths. A future aim is to integrate the device with the thermal control system of a nanosatellite that is under development[2].

The main part of the heat exchange between an object in space and the environment is performed through radiation, which in turn is solely defined by the object surface properties. The modulating device will be attached to the object surface and thus provide a thermal window that can be adapted to the changing conditions in orbit. The key material property is called electrochromism, which means to colour by electricity. Though "colouration" alludes to radiation at visible wavelengths, the modulating ability also exist at infrared wavelengths, which are of main interest here.

The electrochromic material needs to be incorporated with supportive components, such as transparent electrical contacts and an ion conducting electrolyte, to provide electric currents. The technique has been presented earlier in connection with "smart windows"[3-5], and can be found commercially in e.g. windows on building facades[6], rear-view mirrors for cars[7], and motorcycle helmet visors[8]. There exist two main types of electrochromic devices, since the ion conductor can be constituted by a solid polymer[9-11] or an inorganic thin film[12-15]. Polymers in the low pressure space environment have many disadvantages, e.g. they outgas and they are sensitive to ultraviolet (UV) radiation. Thus, only the second type is adaptable to the space environment. The device presented here is rigid and consists solely of inorganic thin films, thus, an all-thin-film (ATF) device. The term "optical" in the thesis title refers to the near-ultraviolet, visible, and

[ii] The platform of a satellite provides mechanical support and power to the scientific instruments, which are termed the payload.

near-infrared wavelength range (0.3-2.5 μm), while “infrared” extends to 50 μm.

Satellite manufacturing includes a large amount of system integration, but the present work has been performed at the component level. No space environmental tests have been conducted, the work is focused on the investigation of the electrical and optical properties of the device and the component materials.

After this introduction, the text is organized according to the following: Chapter 2 gives the background for this work by describing electrochromism and the constituent materials that have been used herein. An overview of related optics of materials is also given. Chapter 3 describes the space environmental aspects and presents some non-electrochromic contemporary thermal control devices. Chapter 4 is devoted to the experimental procedures, including sample preparation and characterization. Chapter 5 presents and discusses the results. The text is ended in Chapter 6 with a summary and conclusion, as well as suggestions for future work.

2 Background

2.1 Electrochromism and devices

Electrochromism means to colour by electricity, and this property can be found among several organic and inorganic compounds[4,5]. This work focuses on inorganic systems.

Inorganic transition metal oxides exhibit electrochromism and can quite easily be deposited as thin films, which is appropriate for device manufacturing. The transition metals are primarily found in the groups 3 to 11 in the periodic table, with partly filled d-bands, and the origin of electrochromism is found in the electron configuration. When forming a transition metal oxide, the Fermi level will be in the band gap for certain elements and in a band for others. In the former case, if the band gap is larger than the energy of incoming radiation we will have a transparent oxide. The metal ion of such a material can be reduced by the insertion of electrons (together with positive ions), and the Fermi level will shift into the next higher band. The material will start to interact with the incoming radiation and become absorbing. For crystalline materials a free-electron condition can arise, and the material will go from transmitting to reflecting. This behaviour is most pronounced at infrared wavelengths.

Going to an absorbing state upon reduction is called cathodic electrochromism, while going to an absorbing state upon oxidation is called anodic electrochromism. The insertion and extraction of ions is called intercalation and deintercalation. Due to the well established work done on electrochromism for optical applications, the terms “bleached” and “coloured” are often seen. However, the former nomenclature describes what really happens at a microscopic level and prevents ambiguity due to the duality of electrochromism.

Thin films of electrochromic materials need mechanical support, and to be modulated they need to be supplied with ions and electrons. A single thin film can be deposited on an electronically conducting substrate. The electrochemical measurements can be performed using an ion containing liquid electrolyte, counter and reference electrodes (see section 4.3.1). To describe a more practical process it is however illustrative to look at a free-

standing electrochromic device. Two basic configurations of such a device are shown in Fig. 2.1, a laminated device for modulation in the visible range Fig. 2.1 a), and an ATF device for IR-modulation Fig. 2.1 b).

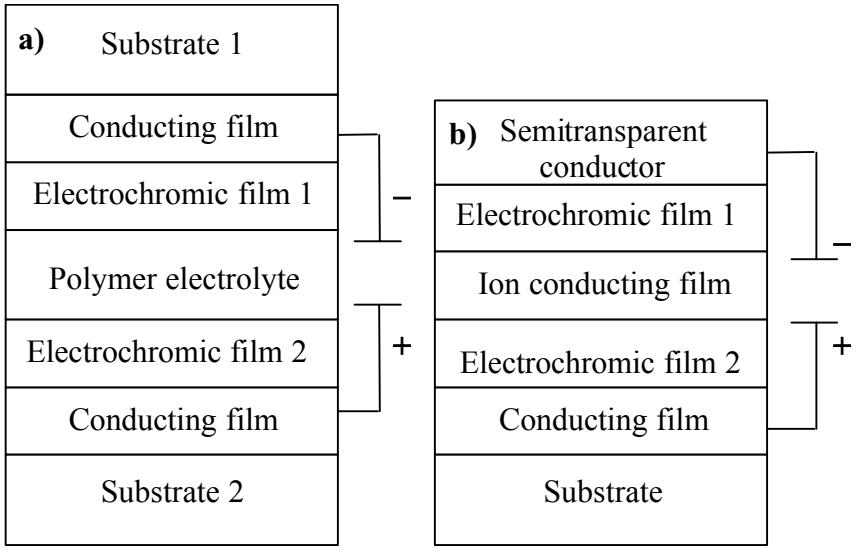

Fig. 2.1: The two basic configurations of electrochromic devices: a) is the conventional laminated device, and b) is the principle of the ATF device for IR-modulation.

The substrates (e.g. glass) of the laminated device in Fig. 2.1 a) are covered with an electrically conducting film. For visible applications this is often indium tin oxide (ITO)[16]. The electrochromic films are deposited onto the ITO. Ions are then incorporated into one of the electrochromic films (say film 1) by, for example, electrochemical insertion (see section 4.3.1). In the case of anodic films ozone treatment can be used to colour them[17]. The two samples are laminated together with the polymer electrolyte, which is permeable to ions, but has a poor electrical conductivity. To modulate the device, a voltage is applied over the electrical conductors, and the ions will move through the electrolyte and into film 2. It is clear that a small ion (such as H^+, Li^+, Na^+, K^+) will facilitate the process, as well as a porous microstructure. Electrons from the outer circuit will now flow into film 2 in order to provide charge neutrality, and the material is reduced. The ions will reside in film 2 until a voltage with reversed polarity attracts them back to film 1. It is therefore appropriate if film 1 is cathodically colouring and film 2 is anodically colouring (or vice versa). Film 2 will then colour upon oxidation as ions are extracted, and when they enter film 1, this will be reduced and colour. The complementary colouring effect will enhance the optical modulation. In cases when film 2 remains transparent upon (de)intercalation, film 1 is called the “active” or “main” layer, and film 2 will then be called the “ion storage” layer.

The ATF device in Fig. 2.1 b) is deposited on a substrate covered with an electrical conductor. The ATF devices intended for thermal control will be attached to a structure that is not infrared transmitting. Thus, the electrical conductor layer can be opaque to infrared radiation, such as an evaporated metal. The film for the ion storage comes next, and the polymer electrolyte will in the ATF be replaced by an ion conducting inorganic thin film. The second electrochromic film, or the active layer, will be deposited onto the ion conducting film. The semitransparent electric conductor on top of the thin film stack can be constituted by a grid shaped evaporated metal layer. The uppermost layer becomes the "front" of the ATF device and must be oriented towards space.

2.2 Materials for devices

2.2.1 General remarks on materials choices

The cathodic electrochromic transition metal oxides are based on Ti, Nb, Mo, Ta and W. The most frequent material as the main layer in devices is WO_3, which is also chosen for all devices in this work. Amorphous and crystalline WO_3 has been used, and are hereafter denoted as a-WO_3 and c-WO_3. The corresponding anodic oxides are based on Cr, Mn, Fe, Co, Ni, Rh and Ir, whereof the most common one for ATF devices is based on NiO. $NiV_xO_yH_z$ was used in the devices here presented.

The ion conduction is carried out by a polymer electrolyte or an inorganic thin film. There is a large variety of polymer electrolytes for laminated devices, and the latter have been reviewed[18]. The laminated device in this work was using an electrolyte consisting of a polymer electrolyte with LiTFSI dissolved in PC (see section 2.2.5). Several inorganic thin film ion conductors have been reported: $LiNbO_3$[12], $LiBO_2$[13] and Ta_2O_5[14,19]. The ATF devices in this work were implemented with a thin film of sputtered ZrO_2, which has previously been reported to be an ion conductor for switchable mirrors[20,21].

Most laminated devices and ATF devices for applications in the visible range use ITO as an electrical conductor[18]. The laminated devices in this work were deposited on glass covered with ITO as a substrate for the ion storage layer, and on Si coated with a grid shaped Al conductor, for the active layer. The infrared reflectance (R) was measured with the radiation incident from the Si/Al substrate side.

Glass covered with ITO can also be used as a substrate for ATF devices for IR applications, but they may as well be implemented with a metallized substrate (since they are asymmetric). An opaque metal layer at the substrate could increase the modulation due to the high reflectance of metals. This

would benefit the emittance modulation in a device where the reflectance is lowered when the active layer (e.g. a-WO_3) is intercalated. If the device reflectance is instead increased upon intercalation of the active layer (e.g. c-WO_3), the emittance modulation would be favoured if the substrate reflectance is low. A device with this type of modulation has been reported[22], with WO_3 as an active layer. A grid shaped pattern of the metal film can be achieved by lithography[23], or by evaporation through a mask (see paper V and VII). The reflectance of the electrical contact at the active layer in an ATF device must always be low, and it is convenient to implement it as a grid[23]. The ATF devices in this work were deposited on glass covered with ITO, and the front electrode was a grid shaped Al conductor (see paper V and VII).

The materials used for the devices in this work will be presented below.

2.2.2 Tungsten trioxide

"Tungsten" is actually the Swedish name for heavy stone, "tung sten". The whitish metal is rare in nature, the average earth supply is 0.0001%[24]. Though it occurs in nature in various oxide compounds, it is the pure tungsten trioxide which is of interest for electrochromic devices. The electrochromic properties of WO_3 films were discovered in 1969[25], and the material has since kept its position as the most studied electrochromic species. WO_3 exhibits cathodic electrochromism, and it goes to an absorbing (a-WO_3) or reflecting (c-WO_3) state after intercalation.

Evaporated bulk WO_3 condenses into a perovskite (cubic) structure where the ideal case consists of perfectly ordered WO_6 octahedra. The octahedra often share corner atoms and/or whole edges[4], and the degree of crystallinity increases with temperature. The structure is quite porous and small alkali ions are easily intercalated and deintercalated. The density starts to increase significantly when the substrate temperature during deposition reaches about 200 °C, and for post annealing about 300 °C. The density of evaporated WO_3 has been reported to be 6.36 and 7.16 g/cm^3 for the monoclinic and hexagonal phase respectively[4]. Intercalation has also been reported to give rise to phase changes in polycrystalline samples[26,27].

The band gap for sputtered a-WO_3 has been reported to vary between 3.0 and 3.4 eV, while the reported value for sputtered c-WO_3 is 2.9 eV[4]. Evaporated a-WO_3, showed an average diffusion coefficient for Li^+ of 10^{-11} cm^2/s and for H^+ 10^{-10} cm^2/s, and the corresponding values for c-WO_3 were 10^{-11} cm^2/s for H^+ and 10^{-12} cm^2/s for Li^+ [4]. The denser structure of the c-WO_3 obstructs the movements of the ions.

2.2.3 Nickel-vanadium hydroxide

Ni and V occur in quite low amounts in nature, the earth supply is estimated to 0.008% and 0.14% respectively[24]. Nickel oxide exhibits anodic electrochromism, i.e., it is transmitting in the as-deposited state and starts to absorb upon deintercalation. The pure nickel metal is magnetic and laborious to sputter from, while a nickel-vanadium alloy with 7% vanadium is non-magnetic[28]. The oxide is still electrochromic and can be used as a device layer complementary to WO_3. The reported optical band gap of nickel oxide is around 4 eV[29]. The addition of hydrogen already at the deposition of $NiV_xO_yH_z$ improves the electrochromic properties, and makes the films more transparent.

X-ray diffractograms for the type of $NiV_xO_yH_z$ used in this work show a cubic structure, the density of the films were 4.6 g/cm^3, and the diffusion coefficient for H^+ was about 10^{-12} cm^2/s [30].

2.2.4 Zirconium dioxide

The earth supply of Zr is estimated to 0.016%, so it is considered to be quite common[24]. ZrO_2 is not an electrochromic material. The low electronic conductivity makes it suitable as an ion conductor in the electrochromic device. The band gap for ZrO_2 has been reported to be 4.1 eV[31], and that of WO_3 is around 3 eV (see section 2.2.2). Since the conduction band of ZrO_2 is at a higher energy than that of WO_3, there will be no available electron states in the ZrO_2 film at the working potential of WO_3. The ions will not be intercalated in the ZrO_2, which makes it a reasonably good ion conductor in devices with WO_3 and $NiV_xO_yH_z$. The diffusion coefficient for both H^+ and Li^+ in ZrO_2 has been reported to be $3.5 \cdot 10^{-13}$ cm^2/s [32]. This is probably the limiting factor for the ion movement in ATF devices (see paper III).

2.2.5 Electrical conductors and polymer electrolytes

The commercial ITO film[33] used in the devices was deposited onto a substrate of Sodalime float glass, and had a thickness of 160 nm. The sheet resistance was 15 Ω per square. The ITO substrate was submitted to the same heating cycle used in the sputtering of c-WO_3. It hardly affected the optical properties at all (see Fig. 2.2).

Aluminium was chosen for the top contacts. It is chemically stable and provides a good adhesion to the WO_3. (Gold has been tried, but seems to diffuse into the oxide layers.) The same type of Al grid was evaporated onto a Si substrate for the laminated device.

The laminated device in this work was constructed with an electrolyte consisting of the salt lithium bis(trifluoromethylsulfone)imide (LiTFSI)

dissolved in propylene carbonate (PC)[iii], with a small additive of polymethyl methacrylate (PMMA)[34].

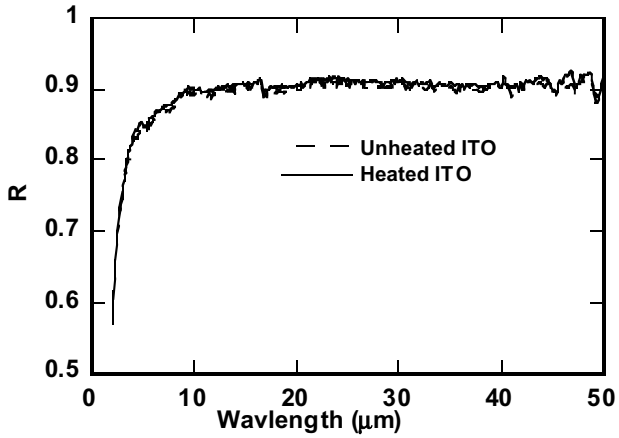

Fig. 2.2: Infrared reflectance spectra of an ITO film on glass that has been heated and an unheated reference sample.

2.3 Performance of electrochromic emittance modulating devices

The initial development of ATF devices concerned window applications, but the benefits and performance of laminated devices appeared to be difficult to compete with. It was in the end of the nineteen nineties that the space community started to be interested in them, due to the growing need of miniaturized thermal control (see chapter 3).

Considering infrared radiation, the use of polymer electrolytes brought great disadvantages. The immediate drawback is the absorption of a conventional electrolyte, and even a thin layer of 20 μm has been reported to reduce the contrast significantly[35]. The electrolyte might outgas in vacuum and cause optically degrading deposition onto the device surface or scientific instruments. Polymers are also known to be UV sensitive. The second substrate of a laminated device might also bring extra weight and hinder part of the radiation to reach the active layer. It seemed like ATF devices were the only possible choice for IR-modulation on spacecraft.

[iii] This is the correct description of the electrolyte used in paper I.

However, a multilayer device has recently been reported, based on an electrochromic solid conducting polymer[36,37]. It exhibits good modulation (see Table 2.1) and has passed initial space environmental tests.

Another device consisting of a WO_3-powder/plastic-matrix hybrid has been reported[38]. This multilayer stack also includes a graphite layer and a $LiCoO_2$ layer. No space environmental tests have been reported and the device exhibits good emittance modulation (see Table 2.1).

An ATF device using c-WO_3 as active layer, and a-WO_3 as ion storage layer has been reported[23]. The a-WO_3 film was thin enough not to be strongly absorbing when intercalated. The ion conducting layer was a-Ta_2O_5. The substrate and top contacts were made either both grid shaped or else only the top contact was a grid, while the substrate contact was continuous. In connection to this device, a coating based on ZnSe was developed for the protection from UV radiation and atomic oxygen[39]. It should be remarked that the extra substrate in laminated devices has an advantage in the mechanical and chemical protection.

The devices in the present work were made in four different configurations with a-WO_3 and c-WO_3 as single active layers or double active layers symmetric around the top contact. Further details can be found in paper VII. Table 1 summarizes the emittance modulation for different electrochromic devices and compares with other non-electrochromic solutions (see section 3.2).

Table 2.1: Emittance of IR-modulating devices at T ≈ 25 °C.

Device	Wavelength range	Low e	High e
a-WO_3 single (Paper VII or ATF I in thesis)	2-50 µm	0.33	0.59
c-WO_3 single (Paper VII or ATF II in thesis)	2-50 µm	0.35	0.60
a-WO_3 double (Dev 3 in paper VII)	2-50 µm	0.50	0.66
c-WO_3 double (Paper VII or ATF III in thesis)	2-50 µm	0.52	0.63
Laminated device (Paper I or sec.5.2.1 in thesis)	2-50 µm	0.56	0.65
ATF_{Franke}[39] *	2.5-40 µm	0.64	0.8
ATF_{Franke}[39] **	2.5-40 µm	0.4	0.58
Laminated device [39]	2.5-40 µm	0.76	0.86
Conducting polymer [37]	2.5-18 µm	0.39	0.79
Hydrous WO_3 powder [40]	2.5-45 µm	0.40	0.70
MEMS louvers[41]	missing	"0.50"	"0.88"
Elecrostatic radiator[42]	missing	"Δε = 0.5"	
Electrophoretic device[43]	missing	"0.29"	"0.8"

* glass| Al-grid | a-WO_3 | Ta_2O_5 | c-WO_3 (active layer) | Al-grid
** glass| Al | a-WO_3 | Ta_2O_5 | c-WO_3 (active layer) | Al-grid

An electrochromic device with WO_3 as an active layer must be oriented away from the sun since the absorption will increase upon intercalation of the WO_3 film, and the surface could get overheated.

2.4 Optics

2.4.1 Emittance and absorptance

For an opaque coating, the spectral absorption $A_\lambda=1-R_\lambda$, while for a semitransparent coating it is given by $A_\lambda=1-R_\lambda-T_\lambda$, where R_λ, and T_λ are the reflection and the transmission respectively. A, R and T are functions of wavelength, λ, or alternatively of the frequency, ω. The solar absorptance, α, and the thermal emittance, e, can be calculated by weighting the measured spectral absorption with the incoming solar radiation S_λ and the blackbody spectrum, $B_{T,\lambda}$ (see Fig. 2.3) for the valid temperature, respectively, and integrating over the particular wavelength interval. The used weight function S_λ was the solar intensity distribution[44] (at Air Mass 1.5). The solar radiation approximates to $B_{T,\lambda}$ at the surface temperature of the sun (ca 6000°C). We assume an opaque material in the thermal infrared. The α and the ε are obtained from:

$$\alpha = \frac{\int_{0.3\mu m}^{2.5\mu m} d\lambda (A_\lambda) S_\lambda}{\int_{0.3\mu m}^{2.5\mu m} d\lambda S_\lambda} \qquad e = \frac{\int_{2\mu m}^{50\mu m} d\lambda (1-R_\lambda) B_{T,\lambda}}{\int_{2\mu m}^{50\mu m} d\lambda B_{T,\lambda}}. \qquad \text{Eq. 1}$$

In this study the emittance refers to the directional one, since it was obtained from Eq. 1 using reflectance data for one angle of incidence. It is an approximation to the hemispherical emittance that should be used for the thermal radiation of a satellite. If the emittance is calculated according to Eq. 1 (and not measured with e.g. an emissiometer) it is important to describe the wavelength range used. The error due to the long wavelength edge cut-off (e.g. Fourier transform infrared spectroscopy, FTIR, is often limited to about 25 μm) will be significant if the sample should be at -50 – +25 °C, not an unlikely temperature on the outer wall of a satellite in orbit. The temperature in Table 2.1 was “room temperature” for all samples (~25°C).

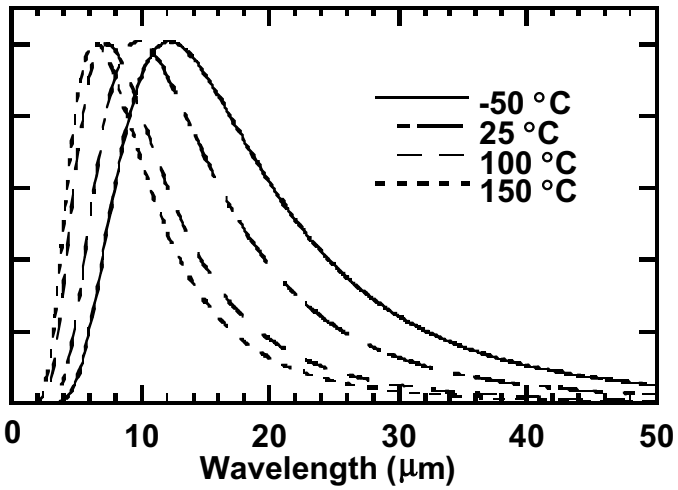

Fig. 2.3: The normalized blackbody spectra for different temperatures.

2.4.2 Material optics

When an electromagnetic (EM) wave strikes a material, the optical response depends on the ability of the charges in the material to polarize. For radiation of optical and infrared frequencies the net response is a superposition of the incoming wave and the secondary one arising from the charges in the material. Metals, semiconductors and insulators behave quite differently to EM radiation, as the classification of them originates from their band structure and electron configuration.

2.4.2.1 Lorentz and Drude models

From the Lorentz and Drude models on the microscopic scale, it is possible to obtain the (measurable) reflectance intensity, R. The outline is that the complex dielectric constant, ε ($\varepsilon=\varepsilon_1+i\varepsilon_2$), is related to the complex refractive index, N ($N=n+ik$), by $N^2=\varepsilon$. The reflectance, R, can then be obtained from N by the Fresnel equations[45].

The Lorentz and Drude models compare an oscillating charge to a classical spring oscillator, where the incident EM wave acts as the driving force. The Lorentz model includes a damping factor and a restoring force and is applied to bound charges (electrons or ions), while the Drude model is suitable to describe free charges (electrons). The Lorentz model can be extended to several oscillators that will be superposed in the equation.

The electrical polarization is related to the electrical field according to

$$P(\omega) = \frac{ne_0{}^2 E(\omega)}{m} \frac{1}{(\omega_0^2 - \omega^2) - i\omega\Gamma} = \varepsilon_v(\varepsilon(\omega) - 1)E(\omega), \text{Eq.2}$$

where n is the charge density, e_0 is the charge, m is the mass ω_0 is the resonance frequency (related to the spring constant in the oscillator analogue), ω is the frequency, Γ is the damping factor and ε_v is the dielectric constant of free space. The middle term is the result when making the ansatz of an incoming plane wave and solving for the oscillator motion. Solving for $\varepsilon(\omega)$ and separating into the real and imaginary parts yields

$$\varepsilon_1(\omega) = 1 + \omega_p^2 \frac{\omega_0^2 - \omega^2}{(\omega_0^2 - \omega^2) + \omega^2\Gamma^2}$$
$$\varepsilon_2(\omega) = \omega_p^2 \frac{\omega\Gamma}{(\omega_0^2 - \omega^2) + \omega^2\Gamma^2} \quad , \quad \text{Eq. 3}$$

where $\omega_p = (ne^2/\varepsilon_0 m)^{1/2}$ is the plasma frequency, and ε_1 and ε_2 in Eq. 3 is the Lorentz dielectric function. For free electrons, the resonance frequency is set to 0, and the equations transform to

$$\varepsilon_1(\omega) = 1 - \frac{(\omega_p\tau)^2}{1 + (\omega\tau)^2}$$
$$\varepsilon_2(\omega) = \frac{\omega_p^2\tau}{\omega(1 + \omega^2\tau^2)} \quad , \quad \text{Eq. 4}$$

where τ is the relaxation time (~the inverse of Γ), and ε_1 and ε_2 in Eq.4 is the Drude dielectric function for free electrons. Further, $\varepsilon = N^2$, which yields

$$\varepsilon_1 = n^2 - k^2 \qquad \varepsilon_2 = 2nk$$
$$n = \left(\frac{1}{2}(|\varepsilon| + \varepsilon_1)\right)^{1/2} \qquad k = \left(\frac{1}{2}(|\varepsilon| - \varepsilon_1)\right)^{1/2}, \quad \text{Eq. 5}$$

and using the Fresnel formalism, the bulk reflected intensity for an opaque material at normal incidence is given by

$$R = \frac{(n_1 - n_2)^2 + (k_1 - k_2)^2}{(n_1 + n_2)^2 + (k_1 + k_2)^2}, \quad \text{Eq. 6}$$

where n_1, n_2, k_1 *and* k_2 are defined in Fig. 2.4 below.

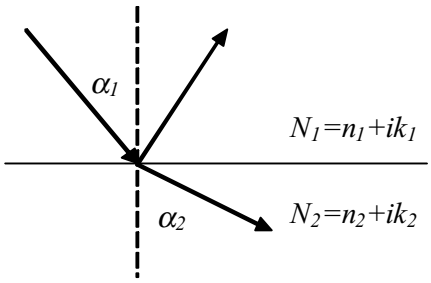

$$N_1 \sin \alpha_1 = N_2 \sin \alpha_2$$

Fig. 2.4: Illustration of Snell's law of refraction at an interface between materials with refractive index N_1 and N_2.

The Drude model describes free electron like materials such as metals, and some transition metal nitrides. The measurements in this work indicate that intercalated c-WO_3 may be Drude-like. For semiconductors and insulators the heavy ions will respond at lower energies. The low frequency signal will be superpositioned on the electron contribution. Bulk ionic materials have a highly reflecting band in the infrared region called the Reststrahlen band. The characteristic parameters correspond to the plasma frequencies of the ions and the resonance frequencies of the ion vibrations, i.e. the longitudinal optical (LO) and transverse optical (TO) phonon resonance frequencies. The latter frequency is found where ε_2 has its maximum. The TO mode defines the low energy flank of the Restrahlen band, where the reflectance increases. The former frequency is called the longitudinal optical (LO) phonon, and it is found when $\varepsilon_1=0$. The LO phonon defines the high energy flank of the Reststrahlen band, where the reflectance decreases. In a thin film a strong absorption is centred at the TO frequency, while absorption at the LO frequency can only be observed at oblique angle of incidence.

2.4.2.2 Thin film optics

The absorption in a slab of thickness d decreases with $e^{-\alpha d}$, so the criterion for a film to be thin is that the optical density, αd, should be of the order of 1, or lower. Further, $\alpha \sim k/\lambda$, hence $kd/\lambda \leq 1$.

The Fresnel formalism is obtained by applying Snell's law of refraction at all interfaces of the thin film model (see Fig. 2.4). This laborious procedure can be found elsewhere[45], only the resulting formulae (for the coherent case and a single film on a semi-infinite substrate) are presented in Eq. 7. Different expressions exist for s and p polarized incident radiation, but are similar. The t and r in Eq. 7 are amplitude coefficients, and their absolute values need to be squared to get the (measurable) intensities T and R. The layer thickness d will enter the equations through the phase shift δ.

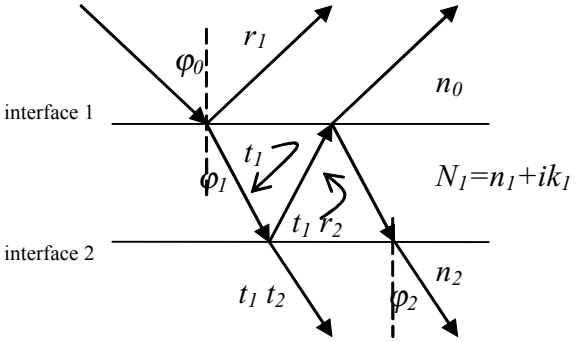

Fig. 2.5: Multiple reflections in a thin film layer of refractive index N_1, the angle of incidence is φ_0, the substrate refractive index is n_2 and the refractive index of the ambient medium is n_0.

$$t = \frac{t_1 t_2 e^{-i\delta_1}}{1 + r_1 r_2 e^{-2i\delta_1}} \qquad r = \frac{r_1 + r_1 r_2 e^{-2i\delta_1}}{1 + r_1 r_2 e^{-2i\delta_1}} \quad . \qquad \text{Eq. 7}$$

$$\delta_1 = \frac{2\pi}{\lambda} N_1 d_1 \cos\varphi_1$$

For s-polarized incident light we obtain[45]

$$T = \frac{n_2 \cos\varphi_2}{n_0 \cos\varphi_0} tt^* = \frac{n_2 \cos\varphi_2}{n_0 \cos\varphi_0} \frac{t_1^2 t_2^2}{1 + 2r_1 r_2 \cos 2\delta_1 + r_1^2 r_2^2}$$
$$, \qquad \text{Eq. 8}$$
$$R = rr^* = \frac{r_1^2 + 2r_1 r_2 \cos 2\delta_1 + r_2^2}{1 + 2r_1 r_2 \cos 2\delta_1 + r_1^2 r_2^2}$$

and for p-polarized incident light we obtain[45]

$$T = \frac{n_0 \cos\varphi_2}{n_2 \cos\varphi_0} tt^* = \frac{n_0 \cos\varphi_2}{n_2 \cos\varphi_0} \frac{t_1^2 t_2^2}{1 + 2r_1 r_2 \cos 2\delta_1 + r_1^2 r_2^2}$$
$$. \qquad \text{Eq. 9}$$
$$R = rr^* = \frac{r_1^2 + 2r_1 r_2 \cos 2\delta_1 + r_2^2}{1 + 2r_1 r_2 \cos 2\delta_1 + r_1^2 r_2^2}$$

The optical constants can be obtained by different measurement techniques and inversion methods that fit models to the spectra. Ellipsometry[46] analyses the magnitude and phase of the polarization shift of

a reflected EM wave. Ellipsometers for infrared wavelengths are not as common as for the visible range. The reflectance (R) and transmittance (T) can be measured with spectrophotometry, and submitted to Kramers-Kronig analysis. This method uses the coupling between the real and imaginary parts of the dielectric function. The optical response for all wavelengths is needed, so the method involves extrapolated values. Alternatively measurements of R and T can be numerically inverted to obtain the real and imaginary parts of N_1 at each wavelength. With R and T, the absorption coefficient, α, can be obtained by the following approximate expression[47]

$$\alpha(\lambda) = \frac{1}{d}\ln\left(\frac{1-R(\lambda)}{T(\lambda)}\right), \qquad \text{Eq. 10}$$

where d denotes the film thickness. Comparison with inversion of the exact Eq. 8 or Eq. 9 gives that the maximum relative error will be less than 15%[47]. Electrochromic materials need conducting layers for the intercalation, so methods that include T measurements are difficult to perform in the infrared. The duality of the optical constants means that there is a need for at least two independent equations to solve. An alternative technique based on only R measurements in the Reststrahlen region has been reported[48]. It uses the fact that R as a function of thickness is a uniquely determined by n and k. The ordinary Fresnel equations are curve fitted to the measured R, as a function of the film thickness.

2.4.2.3 Polarons

A polaron is a quasiparticle constituted by an electron-phonon interaction. The theory was first described in 1933[49], has since then evolved to include a variety of developments, and the field has been thoroughly reviewed recently[50]. Optical absorption by polarons is a feature assigned to WO_3.

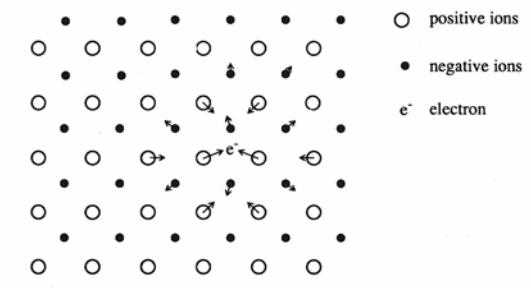

Fig. 2.6: The electron is trapped in the distorted lattice.(After Klingshirn[51])

When an electron (or hole) is inserted into a crystal structure, it can distort the surrounding lattice and create a potential well, in which it gets trapped. It is the system of electron-lattice distortion that constitutes the polaron.

Incoming radiation can excite the electron from the well so it can move to another site and give rise to a new lattice distortion (the former one relaxes). If the extension of the polaron is larger than the lattice constant, it is a large polaron. Free electrons in the conduction band of well ordered crystalline materials can be self-trapped and give rise to large polarons. When c-WO_3 is intercalated, electrons will enter the conduction band, and Paper IV reports on a large polaron-like absorbing state in c-WO_3. If the extension of the polaron is smaller than the lattice constant, the polaron is small. This is often the case for disordered materials, and small polaron absorption in a-WO_3 has recently been reported[52].

The coupling constant determines the size of the polaron. It can be calculated from the polaron mass, and the static and high frequency dielectric constants of the material. Large polarons usually have a coupling constant smaller than one. The coupling constant is given by

$$\varsigma = \sqrt{\frac{E_p 3\pi}{\hbar\omega_L}}, \qquad \text{Eq. 11}$$

were E_p is the polaron binding energy, and $\hbar\omega_L$ is the energy of the LO phonons. E_p can be obtained from

$$E_p = \left(\frac{1}{\varepsilon_0} - \frac{1}{\varepsilon_\infty}\right)^2 \frac{m_p e_0^{\,4}}{96\pi^3\hbar^2\varepsilon_v}, \qquad \text{Eq. 12}$$

where ε_0 and ε_∞ are the static and high frequency dielectric constants respectively, e_0 is the elementary charge and m_p is the effective mass. An approximate (the input parameters are uncertain) value of ς for WO_3 is 4.91 (see paper VI) and the polaron radius is around 6-7 Å[53]. The binding energy, E_p, was calculated to be 179 meV, and the optical absorption peak should be centered at 4 E_p, as predicted by the theory in Paper VI.

3 Thermal control devices

3.1 Heat transfer on small satellites

Heat can be transferred by conduction (within a solid or a non-moving liquid), convection (between a solid and liquid or gas) and radiation (between objects not in contact). Considering an unmanned spacecraft in an earth bound orbit, convection is in most cases negligible. The pressure at a low earth orbit (LEO) at an altitude of 300 km is about 10^{-9} Torr[54]. Between the satellite and the surrounding environment, heat is exchanged by radiation. Heat is led by conduction in the satellite structure, and is transferred by radiation between the internal surfaces. The temperature changes can be calculated by balancing the heat flow for the satellite (often a nodal representation of it) and use the capacitance, a material parameter which is a function of heat flow, mass, time and temperature[55]. The input flows are the radiation from the sun (ca 1390 W/m^2) and the infrared radiation from the earth (ca 237 W/m^2), the fraction of solar radiation reflected by the earth (called the albedo, the average value is 30%) and the dissipated power from the onboard equipment. The output flow is the emitted heat from the satellite that can be calculated by the radiation law

$$q = ee_{env} AF\sigma(T^4 - T_{env}^4), \qquad \text{Eq. 13}$$

where q is the heat flow, e is the hemispherical emittance of the satellite, e_{env} is the hemispherical emittance of the surface the satellite faces, A is the satellite projected area, F is the form factor (that gives how much two surfaces see of each other), σ is the Stefan-Boltzmann constant, T is the temperature for the satellite, and T_{env} is the temperature of the surface the satellite faces[56].

Cost is one of the main driving forces when sending a satellite into orbit. The launch cost is approximately proportional to the mass[1], so there is a good reason to miniaturize satellites. The development has led to a classification of satellites according to mass: Big spacecraft of several tons are just called “satellites”, while the weight of a “microsatellite” is at most

100 kg, that of a "nanosatellite"[iv] is at most 10 kg, and a "picosatellite" weighs 1 kg or less.

The space environment strongly depends on the orbit altitude and the conditions described here refer to a low earth orbit (LEO), which is a typical choice for a nanosatellite[1]. The altitude of a LEO is about 300 km and the orbit time is around 90 minutes, whereof 30 minutes will take place in earth shadow. When satellite dimensions are decreased, the volume and mass decreases faster than the surface area, the latter providing the main possibility to gain or lose heat. The reduced mass will give a lower thermal inertia with a decreased capability to smooth out temperature changes, due to the large heat flow variations in a LEO. Thus, the dependence of the surface properties will be emphasized, and Eq. 13 shows the importance of the emittance. A surface with variable emittance would be most advantageous.

3.2 Non-electrochromic devices

Some non-electrochromic techniques for thermal control devices have been suggested. When comparing the different designs one should know that thermal control systems are divided into active and passive control. Active control draws power which gives the possibility to operate the device, while the passive control is autonomous.

3.2.1 Thermochromic device

Thermochromic materials change their emittance with temperature. The majority of the materials that have been investigated exhibit a modulation not suitable for thermal control as their emittance decreases with increased temperature. However, thin films of $La_xSr_yMnO_3$ have recently been reported to exhibit an emittance that increases with temperature[57]. The change is due to a metal-insulator transition. The emittance could be varied between 0.4 and 0.65 (calculated from reflectance measurements between 1.3 and 27 μm). This material would provide a passive thermal control device.

3.2.2 Micro-electromechanical system louvers

Micro-electromechanical system (MEMS) louvers consist of a silicon substrate with micrometer sized shutters coated with gold[41]. The shutters are configured in an array, and the number of shutters activated can steer the

[iv] The device in this work is intended for a nanosatellite developed by the Ångström Space technology Centre (www.astc.material.uu.se).

resulting emittance. The emittance of the MEMS louvers varied between 0.5 and 0.88. This device would provide active thermal control.

3.2.3 Electrostatic radiator

The electrostatic radiator (ESR) consists of a high emittance surface that will be brought in contact with a low emittance substrate, using a capacitance-like electrostatic force[42]. A good thermal contact is required, and a voltage must be applied to keep the contact state. The change in emittance is reported to be 0.5. This device would provide active thermal control.

3.2.4 Electrophoretic device

The electrophoretic device resembles a liquid crystal display, with suspended flat particles in a fluid. When an electric field is applied the highly reflecting particles align themselves to form a flat reflective surface. The emittance modulation was reported to vary between 0.29 and 0.80[43], however, no information is given on how it was measured. The electrophoretic device would provide active thermal control

3.2.5 The paraffin phase transition device

The paraffin phase transition device uses the solid-to-liquid phase transition of paraffin to bring a high emittance surface in contact and non-contact with the substrate[58]. The development status of this device is (2003) at the mechanical level and the investigation of the spectral properties are yet to come. The paraffin phase transition device would provide active thermal control

4 Experimental

4.1 Sample preparation

4.1.1 Thin film deposition

Thin metal oxide films can be manufactured by several deposition techniques, usually grouped into physical vapour deposition (PVD) and chemical vapour deposition (CVD), and additionally some other methods based on solutions. In PVD, free atoms from a solid target are released for example by ion bombardment (sputtering) or heating (evaporation). The atoms can react or mix with other substances before or at the deposition on the substrate. The CVD process comprises the mix of gases of the materials to be deposited, often at an elevated temperature. Examples of techniques based on solutions are: Sol-gel deposition, anodization, screen printing and electroplating. The deposition methods used in this work were sputtering and evaporation.

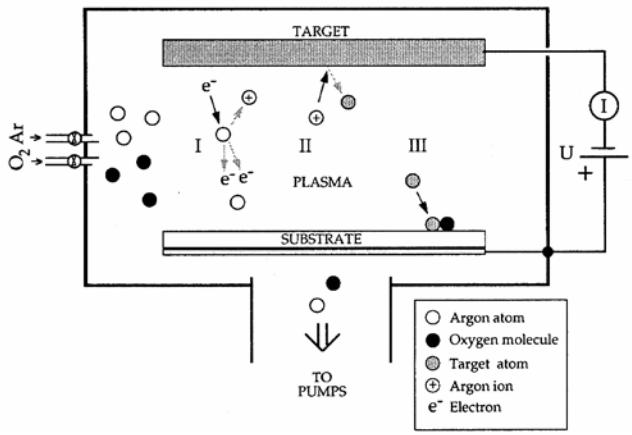

Fig. 4.1: Illustration of the DC glow discharge sputtering system. (After Veszelei[59].)

Sputtering[60,61] provides many advantages such as control of the thickness and structure, a good adhesion to the substrate and a large choice of materials to work with. The process takes place inside a vacuum chamber (see Fig. 4.1) and the substrate is placed on a substrate holder that can often be heated. The target (the cathode) is a solid piece of the material to be deposited and it should be electrically isolated from the rest of the chamber (the anode) including the sample. A high voltage is applied between the target and the sample and an inert gas (the working gas), like Ar is led into the chamber. The voltage should exceed the breakdown potential of the working gas so that electrons emitted from the cathode will ionize the gas and a glow discharge is built up. The argon ions proceed to the target where they knock out atoms and secondary electrons. The atoms can deposit on the substrate, possibly preceded by forming an oxide or a nitride etc. with a provided reactive gas. The electrons will ionize new argon atoms, and the plasma is sustained. A DC field can be used in case of conducting targets. A magnetron attached to the cathode can bend the electron trajectories and elongate their path in the chamber, thus the rate of ionization is increased. This work used a Balzers UTT 400 system for reactive DC magnetron sputtering. The background pressure was 10^{-6} Torr, and the purities of the argon, oxygen and hydrogen gases were 99.998%. The target diameters were 5 cm, and the metal purities were 99.7% for Ni, 99.95% for NiV, 99.9% for Zr and 99.99% for W. The sputter parameters for the different samples can be found in Table 4.1. The distance between target and substrate was 13 cm.

Evaporation is a more direct process that was used for the grid deposition. The instrument was an Edwards E306 A evaporation system. A curled thread of Al is placed in a tungsten crucible (or helix) and submitted to resistive heating. The sample is placed on a substrate holder above the evaporation source. The background pressure was 10^{-6} Torr, and the distance between the sample and the tungsten crucible was about 15 cm.

4.1.2 The sample preparation procedure

Two categories of samples have been manufactured, single thin films and ATF devices. The substrates were glass covered with ITO and Si with an evaporated Al grid. The ITO substrates were submitted to an ultrasonic bath in a heated solution of ethanol and deionized water before deposition. The Si wafers had been stored in a clean-room and washed in ethanol before deposition.

The single films where masked with teflon tape to prepare for thickness measurements.

For the laminated devices, $NiV_xO_yH_z$ was deposited on the ITO covered glass, and WO_3 was deposited on the Si/Al-grid substrate. The double substrate devices were laminated inside an Ar-filled glove box, using a

vacuum chamber to extinguish gas bubbles in the electrolyte. The edges of the device were then sealed with silicon glue before it was submitted to air.

When preparing the ATF devices, the samples were taken out of the sputtering chamber between the deposition of the different materials. Films of $NiV_xO_yH_z$, ZrO_2 and WO_3 were deposited by sputtering on the ITO coated substrates. A frame shaped shadow mask was used during deposition to avoid short circuits between the different layers. An Al grid was then evaporated on top of the thin film stack using a shadow mask. Some of the devices got a second layer of WO_3 over the Al grid.

Hydrogen was inserted in the $NiV_xO_yH_z$ films (for the ATF devices) in the sputtering process, so the as-deposited films were in the bleached state. The WO_3 film for the laminated device was pre-charged with liquid Li-electrolyte (described in section 2.2.5) before lamination.

The sputtering parameters of the samples presented in this section are found in Table 4.1. The section where each film is used is referred to in the table.

Table 4.1: The sputtering parameters and film thicknesses for the different films and devices presented in chapter 5. The p is the background pressure, T is the substrate temperature, P is the applied power, f is the gas flow and d is the film thickness.

Section	Film	Substrate	p (mtorr)	T (°C)	P (W)	f Ar/O_2/H_2 (ml/min)	d (nm)
Single films							
5.1.1	a-WO_3	Glass/ITO	30	r*	275	7/15/-	1270
	c-WO_3	Glass/ITO	30	350	275	7/15/-	1450
5.1.2	a-WO_3	Glass/ITO	30	r	275	7/15/-	745
	c-WO_3	Glass/ITO	30	350	275	7/15/-	460
Devices							
5.2.1							
*lam**	$NiV_xO_yH_z$	Glass/ITO	35	r	200	2.7/10/-	800
	a-WO_3	Si/Al grid	30	r	275	7/15/-	700
5.2.2							
ATF I	$NiV_xO_yH_z$	Glass/ITO	30	r	200	50/2/1/-	380
	ZrO_2		28	r	200	30/1.4/-	235
	a-WO_3		30	r	275	7/15/-	380
ATF II	$NiV_xO_yH_z$	Glass/ITO	30	r	200	50/2/1	390
	ZrO_2		28	r	200	30/1.4/-	235
	c-WO_3		30	350	275	7/15/-	380
ATF III	$NiV_xO_yH_z$	Glass/ITO	30	r	200	50/2/1	340
	ZrO_2		21	r	200	30/2.5/-	590
	c-WO_3 L1		30	350	275	7/15/-	380
	c-WO_3 L2		30	350	275	7/15/-	380

* r = rom temperature, lam = laminated

4.2 Structure and composition

4.2.1 Profilometry

The thickness of the films in this work was measured by a Tencor Alpha Step 200 profilometer, with a vertical resolution of 5 Å. A mechanical diamond tip stylus is moved over the film edge and the height is recorded. Several measurements per sample were performed to average over variations in the film thickness.

4.2.2 Rutherford backscattering spectrometry

Samples of WO_3 prepared with identical sputtering parameters to those used in this work, were submitted to Rutherford backscattering spectrometry[62] (RBS) to obtain the elemental composition and depth profiling. This is a non-destructive analysis technique where the material is submitted to a perpendicular bombardment of high energy alpha particles (about 2-3 MeV). The energies of the backscattered particles depend on the mass of the scattering nuclei and their depth within the sample.

The density of the films was determined by RBS to be 5.60 and 6.44 g/cm^3 for the a-WO_3 and c-WO_3 film respectively[27]. The elemental composition was stoichiometric within experimental uncertanities.

4.2.3 X-ray diffraction

X-ray diffraction[63] (XRD) can be used to identify a material and give information about the phase, lattice stress, texture orientation and grain size. It is based on the constructive interference between x-rays reflected at different atomic planes. By varying the angle between the incident and diffracted beam and recording the diffracted radiation, a chart with material and phase specific peaks is achieved. In this work the method has been used to determine the grain size. It can be calculated by inserting the full-width-half-maximum of the intensity peak, in Sherrer's formula[63].

Sputtered WO_3 films used in this work were submitted to X-ray diffraction using a Siemens D5000-unit with CuK_α radiation of 1.54 Å. During sputtering, the substrates where kept at temperatures ranging from 100 to 350 °C. Fig. 4.2 shows that diffraction peaks pertinent to the monoclinic structure start to appear at 250 °C and can be clearly identified at 350 °C. Even the spectra without the characteristic peaks may originate from samples with a crystal structure, but with a grain size below the instrument resolution. Such samples are hereafter referred to as x-ray amorphous WO_3 (a-WO_3). The background level, with a hump between 20 and 30 degrees originates from the glass substrate. The grain size of the polycrystalline WO_3

(c-WO_3) was determined by Scherrer's formula[63] to 30 nm. (All individual peaks in Fig. 4.2 are not resolved, and the grain size calculation was done on a main peak diffractogram with higher resolution, not shown here.)

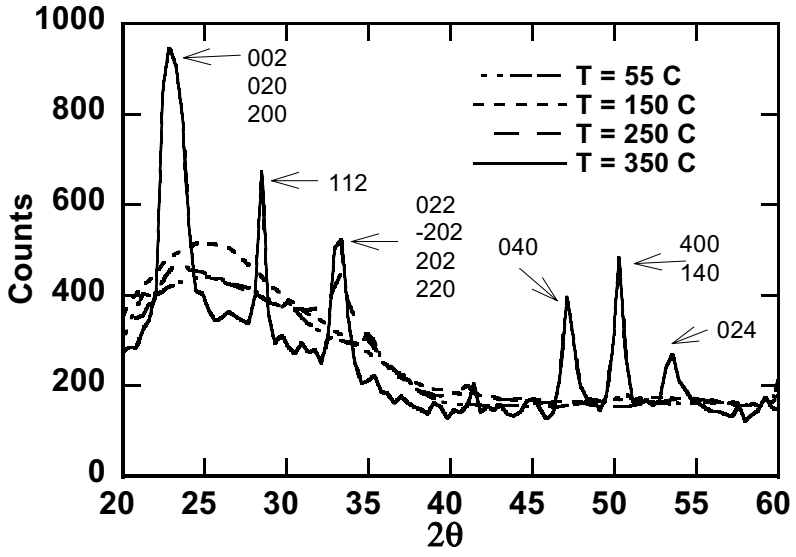

Fig. 4.2: X-ray diffractograms for monoclinic WO_3 sputtered at different substrate temperatures, shown in the figure. The indexed peaks are those of the monoclinic phase

4.3 Electrochemical and optical measurements

4.3.1 Electrochemical measurements

To intercalate the mono-layered samples, a three-electrode-setup with liquid electrolyte was used (see Fig. 4.3). Li foil was used for the counter and reference electrode (CE and RE respectively), while the working electrode (WE) was the sample itself.

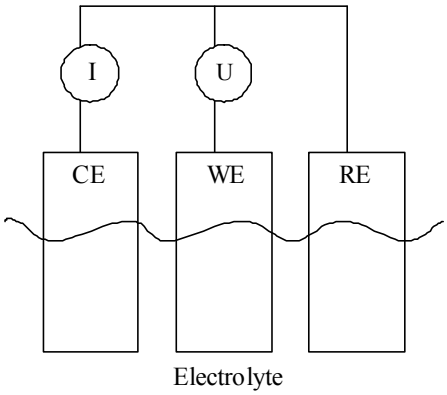

Fig. 4.3: Schematic picture of a three-electrode set-up with counter electrode (CE), working electrode (WE) and reference electrode (RE) in a liquid electrolyte.

Lithium is highly reactive with humidity, so the experiments where carried out inside an Ar-filled glove box with less than 4 ppm of water. The electrolyte was 1M lithiumperchlorate ($LiClO_4$) salt dissolved in propylene carbonate (PC). A voltage is applied between the WE and the RE, while the current is measured between the WE and the CE. The electrochemical recordings were done with an ECO Chemie Autolab/GPES interface.

Before the optical measurements the samples were taken out of the glove-box and washed in ethanol. The loss in transmission after a certain elapsed time for a-WO_3 can be seen in Fig. 4.4. After the optical measurements the remaining charge was deintercalated and measured, and this is referred to as the amount of charge during the optical measurement. The charge loss found by this procedure was about 15 %.

The Li/W ratio was calculated by

$$x = \frac{Q_{Li} \cdot M}{e_0 A d \rho \cdot N_A}, \qquad \text{Eq. 14}$$

where Q_{Li} is the inserted charge, M is the molar mass, e_0 is the elementary charge, A is the intercalated area, d is the film thickness, ρ is the film density and N_A is Avogadros constant..

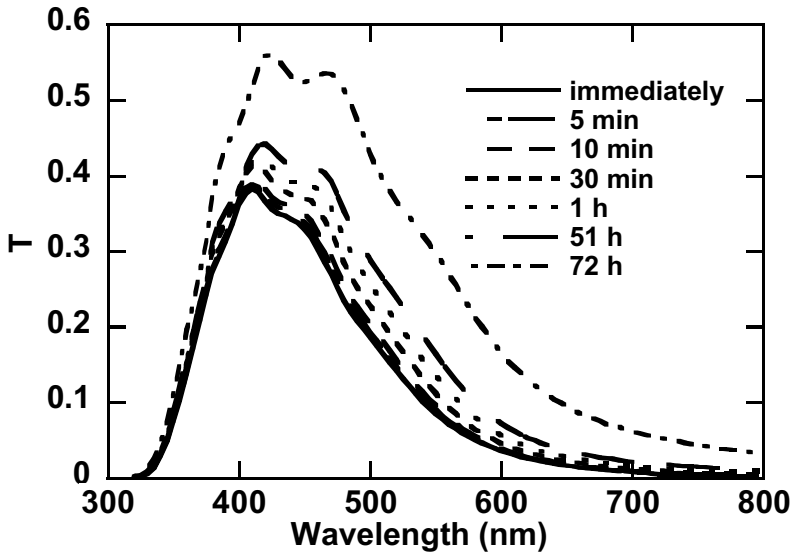

Fig. 4.4: Transmission loss due to leakage after certain elapsed times for an intercalated WO_3 film.

Cyclic voltammetry (cv) is a method where the voltage is swept while the current is measured. The method was used to find the limiting potentials for the samples, and pre-cycle the samples to ensure reversible conditions during the following measurements. Galvanostatic ampereometry (ga) is a method where a constant voltage is applied and the current is measured. The method was used to intercalate the samples with a certain amount of charge before the optical measurements were done. The deintercalation was done with ga as well.

The devices were cycled in ambient atmosphere using the same techniques, but with the reference and working electrodes short circuited. Devices have only two electrodes and they were used as WE and CE.

4.3.2 Optical measurements

The infrared optical measurements were recorded with a Perkin-Elmer 983 spectrophotometer. This is a double beam instrument with a rotating mirror operating in the range 2 to 50 μm. Sputtered gold mirrors were used as references, assuming that the reflectance was 100%, which yields an absolute error of 1–2 percent. However, the main concern in this work is the relative change for different intercalation levels. The angle of incidence was around 25 ° [v]. The incident infrared radiation was to a good approximation unpolarized. It was verified in several cases that the measured R

[v] Note that ”near normal” is unfortunately used in paper I and II.

corresponded to the average of the R-values obtained for s- and p-polarized radiation. To improve the signal to noise ratio, an air dryer was used.

The area of the active WO_3 layer was smaller than the incoming beam, so delimiting masks were used when measuring the ATF devices. The data correction was done according to

$$S_{sample} = \frac{S_{measured,sample+mask} - S_{measured,mask}}{S_{measured,reference} - S_{measured,mask}} \quad \text{Eq. 15}$$

The near-normal T and R measurements in the near-ultraviolet/visible/near-infrared wavelength range were done with a Perkin-Elmer Lambda 9 spectrophotometer. This is a single beam instrument operating in the range 300 to 2500 nm. The light is collected in an integrating sphere covered with $BaSO_4$, which is also used as a reflectance reference. The R data were corrected for the reflectance of $BaSO_4$ [64] afterwards.

4.3.3 In-situ electrochemical and optical measurements

Electrochemical and optical measurements were recorded in-situ for the ATF devices. The samples were connected to the ECO Chemie Autolab/GPES interface when placed inside the spectrophotometer measurement compartment. A voltage was applied to intercalate either of the electrochromic layers, and when a certain amount of charge had been transferred, an optical spectrum was recorded. The voltage was constant during the recording. The order of the measuring time was much smaller than the total intercalation time, and the current density decreases when the films approach a fully intercalated or deintercalated state. The intermediate values are considered less important.

5 Results

5.1 Optical measurements on single films

5.1.1 Measurements in the infrared range

Single films of WO_3, deposited onto ITO-covered glass, were submitted to Li-intercalation, as described in section 4.3.1. The Li/W ratio calculated by Eq. 14, is denoted by x.

The infrared reflectance at different intercalation levels for a-WO_3 (1270 nm thick) and c-WO_3 (1450 nm thick) films are shown in Fig. 5.1 and Fig. 5.2[vi] respectively. For the as-deposited films there is a well defined absorption around 17 μm, located in the Reststrahlen region of WO_3. This is due to the interaction of electromagnetic waves with the main TO phonon mode in WO_3. The shift as a function of intercalation level of this absorption is probably due to interference effects. The ITO contributes to the high reflectance at wavelengths beyond 20 μm, especially for thin films. Interference effects are clearly seen in the wavelength range 2 – 10 μm. Features from OH and HOH bands around 3 and 6 μm are visible for the as-deposited film in Fig. 5.1. The c-WO_3 film in Fig. 5.2 exhibits a clear free-electron like behaviour at intercalation levels $x \geq 0.25$. For the a-WO_3 film in Fig. 5.1 the interference fringes at wavelengths below 10 μm are smoothed out at high intercalation levels.

In Fig. 5.3 the reflectance curve of the a-WO_3 film at $x = 0.35$ is compared with the reflectance curve of the c-WO_3 film with $x = 0.10$. The reflectance curves of the two films are similar. A first impression may be that the a-WO_3 film is going towards a free-electron like state, but the reflectance does not increase with intercalation level at long wavelengths, hence interference effects are still dominant in the spectrum. The intercalation of a-WO_3 was actually continued to $x = 0.56$, but then the

[vi] Note that some graphs in this chapter with a logarithmic wavelength scale for clarity, are found with a linear scale in the papers.

intercalation was not reversible. The reflectance spectrum is similar to that for x = 0.35, but at a slightly lower level as seen in Fig. 5.3.

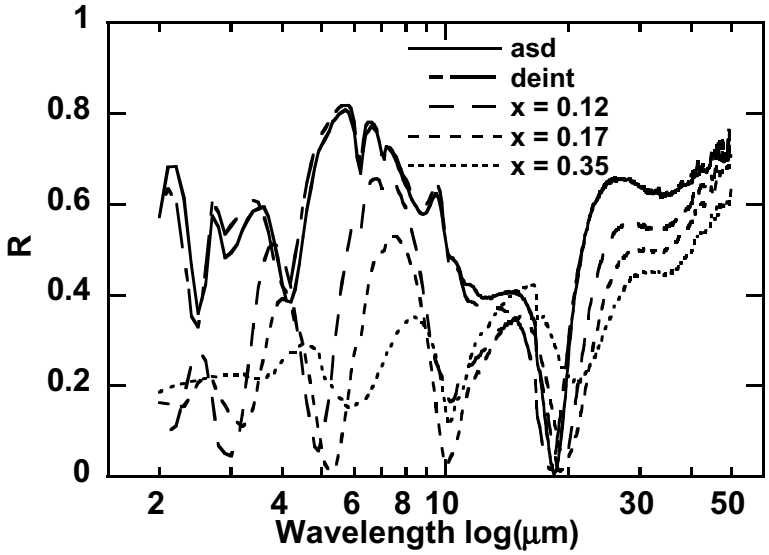

Fig. 5.1: Infrared reflectance of a 1270 nm thick a-WO_3 film at different intercalation levels x, including the as-deposited (asd) and deintercalated (deint) states. The angle of incidence was 25°.

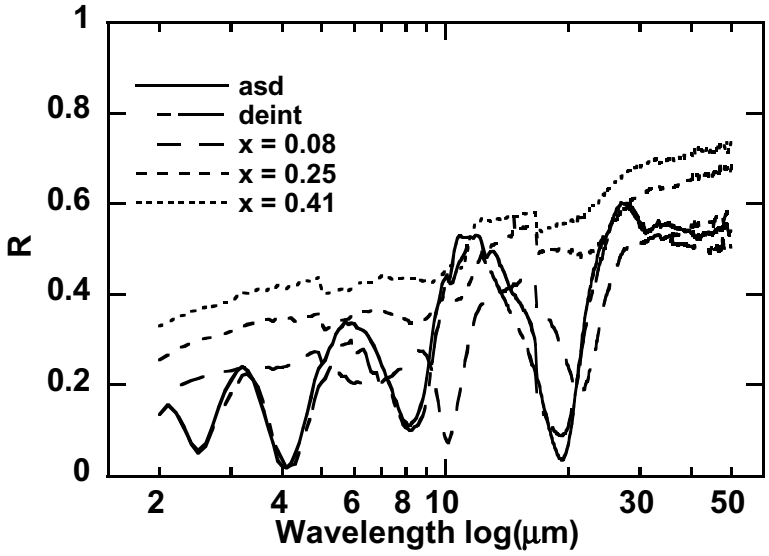

Fig. 5.2: Infrared reflectance of a 1450 nm thick c-WO_3 film, at different intercalation levels x, including the as-deposited (asd) and deintercalated (deint) states. The angle of incidence was 25°.

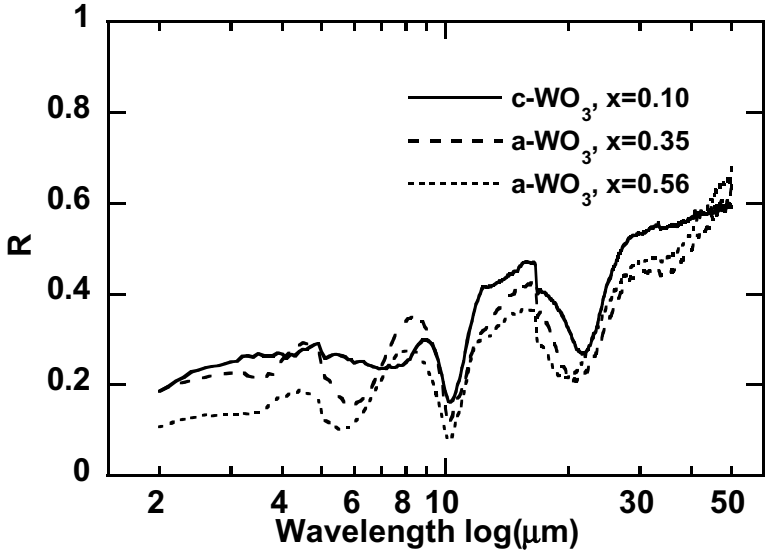

Fig. 5.3: Infrared reflectance of c-WO_3 and a-WO_3 films at the intercalation levels x = 0.10 and 0.35, as well as 0.56, respectively. The films were the same as in Fig. 5.1 and Fig. 5.2.

The calculated emittance for the a-WO_3 films, c-WO_3 films and a nanocrystalline WO_3 film[65] (2800 nm thick) is shown in Fig. 5.4. It can be seen that the emittance of c-WO_3 is going through a maximum around x = 0.05, thus, the largest emittance modulation is not between the lowest and highest intercalation levels. The maximum is most likely due to that the interference fringes shift towards longer wavelengths with increasing x, and there is a reflectance minimum approaching 10 μm where the blackbody curve has its maximum at 25 °C. A more extended maximum in the emittance modulation of the a-WO_3 film is also seen, which corresponds to interference effects as discussed above. From the features of Fig. 5.4 it is clear that a device could be built with a-WO_3 and c-WO_3 so that ion intercalated c-WO_3 yields a low emittance at the same time as deintercalated a-WO_3 will yield a low emittance, in a complementary manner. A device with this design has been reported,[23] with a c-WO_3 film as the active layer and a-WO_3 as the ion storage layer. Both films where 160 nm thick. In paper II it is shown that the reflectance modulation for so thin films is quite small, and it was supposed that the a-WO_3 film in the reported device was sufficiently thin to be inactive. Hence, the devices of Franke et al.[23] were probably modulated by the reflectance change of the c-WO_3 film and the interference effects in the total thin film stack. The WO_3 films in devices presented in paper VI were twice as thick, and these devices exhibited a higher emittance modulation. In this case the interference could be used to

enhance the modulation. A multilayer thin film device will of course get additional interference from the remaining layers.

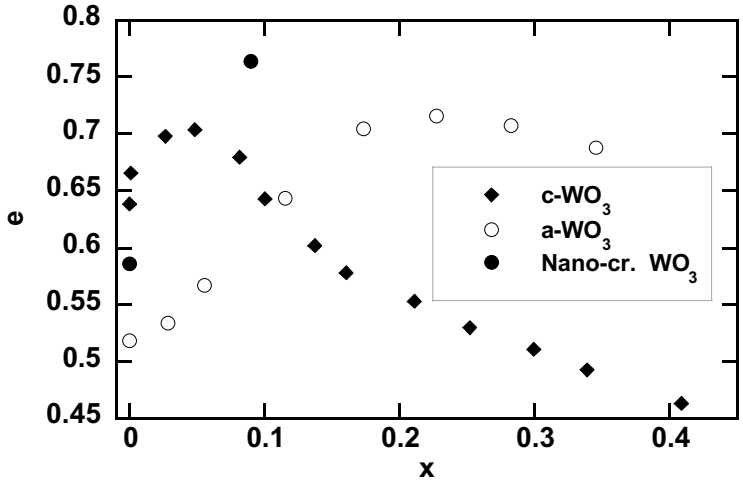

Fig. 5.4: Emittance calculated from reflectance spectra, for a c-WO_3 film of thickness 1270 nm, an a-WO_3 film of thickness 1450 nm and a nanocrystalline WO_3 film of thickness 2800 nm.

5.1.2 Measurements in the near-ultraviolet/visible/near-infrared range

Single films of WO_3, deposited onto ITO-covered glass, were submitted to Li-intercalation, and x was calculated according to Eq. 14. The R and T spectra were measured in the wavelength range 300 – 2500 nm at different intercalation levels. The transmission for a c-WO_3 film of thickness 460 nm at different x can be seen in Fig. 5.5 a), and the corresponding reflectance spectra are shown in Fig. 5.5 b). The transmission of the c-WO_3 film in Fig. 5.5 a) is reduced to almost zero in the NIR range upon intercalation, while it is still around 0.4 in the UV/VIS range. A possible application for a device with this property is discussed in section 5.2.2. The transmittance spectra of an a-WO_3 film of thickness 745 nm, shown in Fig. 5.5 c), do not exhibit this selective property to the same extent. The reflectance of the c-WO_3 film in Fig. 5.5b) increases with x with a Drude-like appearance in the NIR range, which is not seen in the reflectance spectra for the a-WO_3 film in Fig. 5.5 d). When electrons enter the conduction band they interact with the phonons and form polarons, which is believed to give rise to absorption at NIR wavelengths. When the polaron states start to overlap, free electron behaviour is expected.

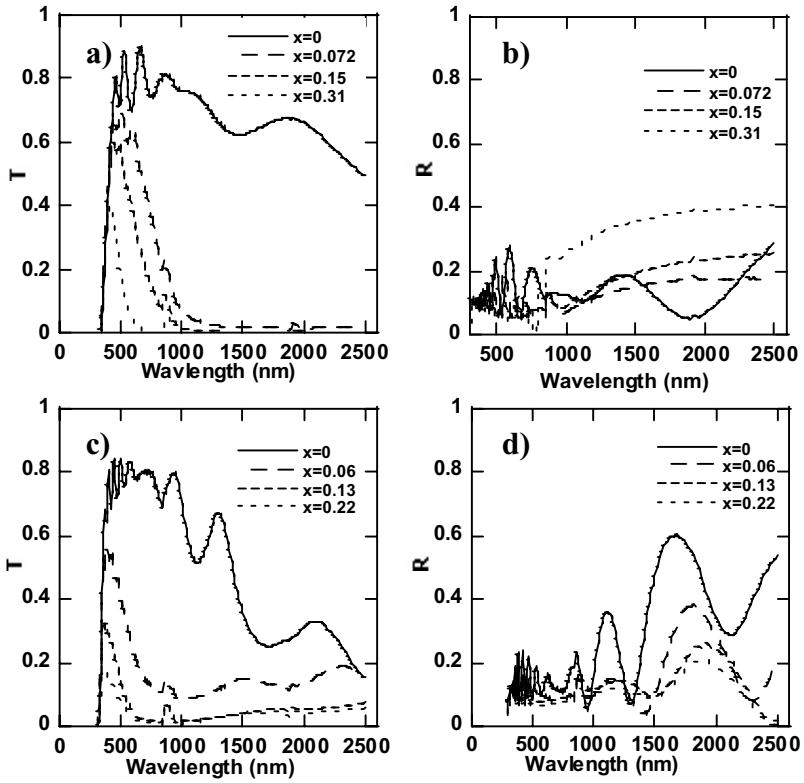

Fig. 5.5: Optical spectra in the wavelength range 300 – 2500 nm showing a) transmittance and b) reflectance of a Li-intercalated c-WO_3 film of thickness 460 nm, and c) transmittance and d) reflectance of a Li-intercalated a-WO_3 film of thickness 745 nm.

The polaron absorption in c-WO_3 at low intercalation levels will now be studied. The absorption coefficient of a c-WO_3 film is shown Fig. 5.6 for the as-deposited state and for low intercalation levels. Paper VI compares the absorption coefficient of c-WO_3 with large polaron theory. It should be noted that the coupling constant in this comparison is 4.91 (> 1), and the radius of the polaron is 6-7 Å[53] (which is of the order of the lattice constant for monoclinic WO_3), so the polaron itself is small or intermediate. These values are consistent with the discussion in section 2.4.2.3. In particular the observed absorption peak is situated at an energy of about four times the polaron binding energy.

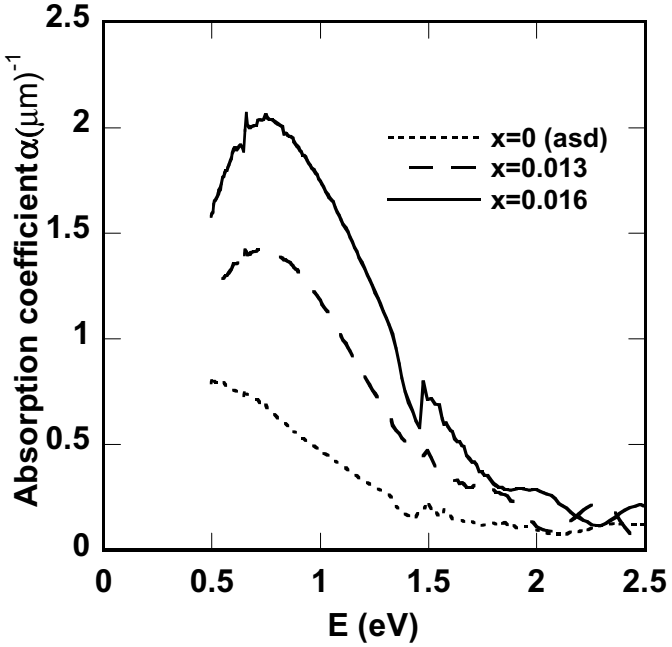

Fig. 5.6: Near-infrared absorption coefficient of c-WO_3 films for the as-deposited state and at two low intercalation levels (given as Li/W ratios x).

5.2 Optical measurements on devices

5.2.1 Laminated device

Measurements on a laminated device will now be presented. The active layer was WO_3 (700 nm), deposited on Si with an evaporated Al-grid (110 nm) and the ion storage layer was $NiV_xO_yH_z$ (800 nm), deposited on ITO covered glass. The two halves were laminated with an electrolyte consisting of LiTFSI in PC and PMMA (see section 2.2.5). Thus, the configuration of the device was glass | ITO | $NiV_xO_yH_z$ | polymer | a-WO_3 | Al-grid | Si. The device was submitted to pre-cycling with CV for 5 cycles. A voltage of about −3 V was applied at the Al contact and a visual inspection determined when it was distinctly coloured. The voltage was removed, and the infrared reflectance was measured with the Si/Al grid substrate facing the incident radiation. The Si/Al-grid substrate was also measured for comparison. The deintercalation was done with +3V. The spectra of the intercalated and deintercalated state can be seen in Fig. 5.7. The calculated emittance varied between 0.56 and 0.65 for the deintercalated and intercalated states

respectively. The low modulation is most likely due to the thick layer of absorbing electrolyte.

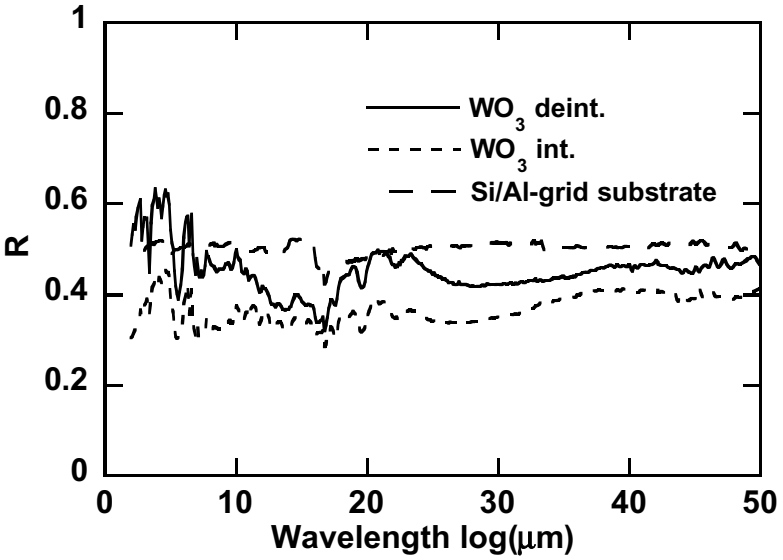

Fig. 5.7: Infrared reflectance spectra of a laminated glass | ITO | $NiV_xO_yH_z$ | polymer | a-WO_3 | Al-grid | Si device with the WO_3 film in intercalated and deintercalated states. The reflectance of the Si/Al-grid substrate is shown for comparison.

5.2.2 All-thin-film devices

Measurements on three types of ATF devices will be presented. The first device, called ATF I, had the structure shown in Fig. 2.1 b) with a-WO_3 (380 nm) as an active layer, ZrO_2 (235 nm) as ion conductor and $NiV_xO_yH_z$ (390 nm) as ion storage layer. The top contact was an evaporated Al-grid with a thickness of 110 nm (this is the same for all ATF devices described here). The second device, called ATF II, had the structure of Fig. 2.1 b), with c-WO_3 (390 nm) as active layer, ZrO_2 (235 nm) as ion conductor and $NiV_xO_yH_z$ (380 nm) as ion storage layer. The third device, called ATF III, had two layers of a-WO_3 embedding the Al-grid (see Fig. 5.8), each with a thickness of 340 nm. The ion conduction layer was ZrO_2 (580 nm) and the ion storage layer was $NiV_xO_yH_z$ (340 nm).

A voltage of –/+5 V was applied at the Al grid during intercalation/deintercalation for all devices.

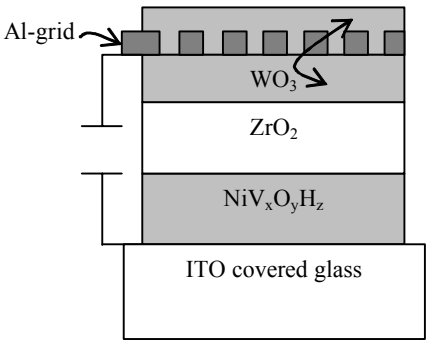

Fig. 5.8: Schematic sketch of the ATF III device with an embedded Al-grid.

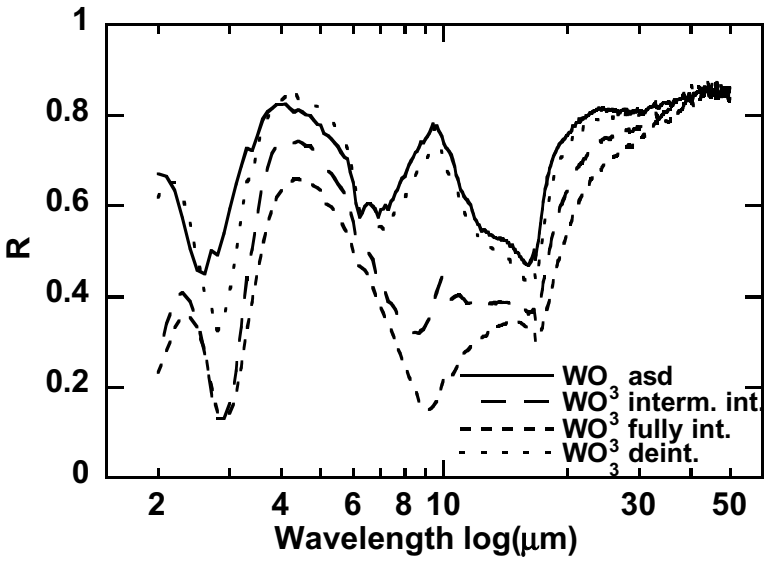

Fig. 5.9: Infrared reflectance spectra of an all-thin-film glass | ITO | $NiV_xO_yH_z$ | ZrO_2 | a-WO_3 | Al-grid device with a single layer of a-WO_3. The spectra were taken when the a-WO_3 film was as-deposited, intermediately intercalated, fully intercalated and deintercalated, as specified in the figure. A voltage of –/+5 V was applied at the Al grid during intercalation/ deintercalation.

The reflectance spectra for the ATF I device, when the a-WO_3 film was as-deposited, intermediately intercalated, fully intercalated and deintercalated, are shown in Fig. 5.9. The device was not pre-cycled with CV, however, the deintercalated state in Fig. 5.9 was taken after 10 cycles and exhibits good agreement with the as-deposited curve. There is a dip in the reflectance around 7 μm, most likely due to interference. As the WO_3 film is intercalated the fringes shift towards longer wavelengths; this leads to the large modulation around 9 μm. At wavelengths beyond 20 μm, there is

very little modulation. The calculated emittance modulation for this device was from 0.33 (deintercalated state) to 0.59 (intercalated state).

The corresponding spectra for the ATF II device with c-WO_3, can be seen in Fig. 5.10. The infrared reflectance of the mono films of c-WO_3 increased with intercalation, but the ATF II device shows a lowered reflectance when intercalated. The intercalation was characteristically slow compared to the device with the a-WO_3. The current density during the intercalation process is shown in Fig. 5.11 for the ATF I (a-WO_3) and ATF II (c-WO_3) devices respectively. After an initial transient decay a peak is seen in Fig. 5.11 a) with a subsequent decrease in current density. The peak has been shown by Frenning et al.[66] to be due to the ionic current through the device. As discussed in paper III, the ionic current density will decrease again as the ions pile up at the Al electrode. This is indicated with an arrow in Fig. 5.11 a). For the ATF I device this occurs after approximately 1000 s, while in ATF II this has not yet occurred after 3000 s. This indicates that the structure of the WO_3 film in the ATF II device is denser than the one in ATF I.

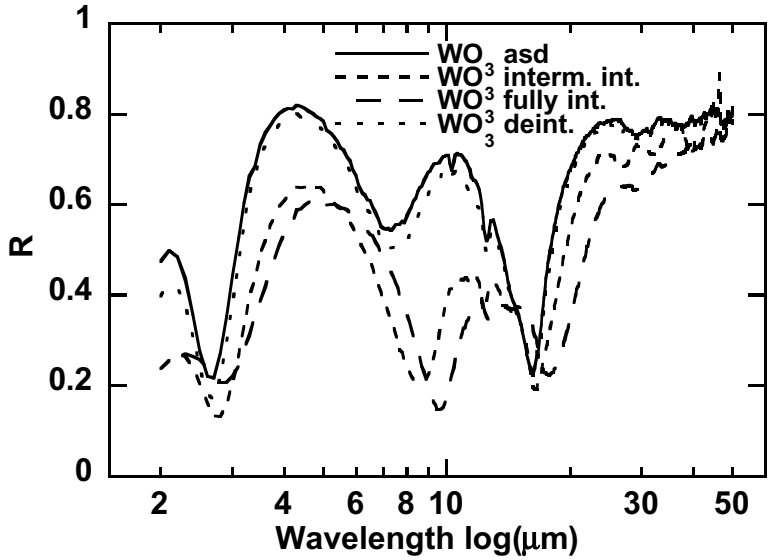

Fig. 5.10: Infrared reflectance spectra of an all-thin-film glass | ITO | $NiV_xO_yH_z$ | ZrO_2 | c-WO_3 | Al-grid device with a single layer of c-WO_3. The spectra were taken when the WO_3 film was as-deposited, intermediately intercalated, fully intercalated and deintercalated, as given in the figure. A voltage of –/+5 V was applied at the Al grid during intercalation/ deintercalation.

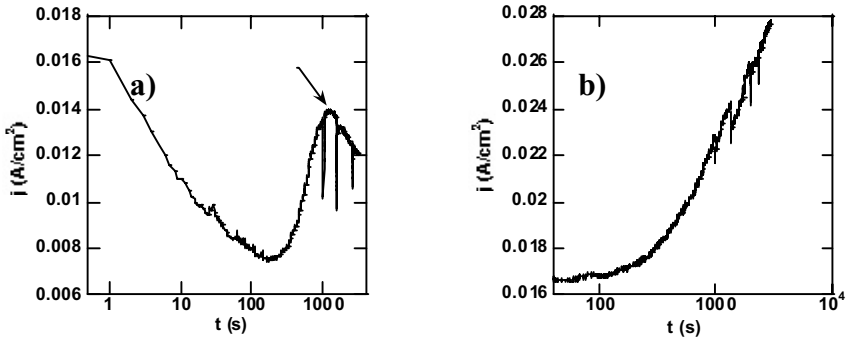

Fig. 5.11: Current densities during intercalation of an all-thin-film device with a) a-WO_3, and b) c-WO_3. The arrow in a) indicates when the ions have travelled to the Al contact. This feature is not seen in the device with c-WO_3 in b). A voltage of –/+5 V was applied at the Al grid during intercalation/ deintercalation.

The ion diffusion coefficient can be obtained from[32]

$$D = \frac{L^2 kT}{te_0 V}, \qquad \text{Eq. 16}$$

where L is the distance between the $NiV_xO_yH_z$ film and the WO_3/aluminium interface, k is the Boltzmann constant, T is the absolute temperature, t is the time for the peak, e_0 the elementary charge and V the voltage. The time for the peak equals 1220 s, L equals 805 nm, including half of the $NiV_xO_yH_z$ thickness (see Table 4.1), T equals 293 K and the applied voltage is −5 V, D is then obtained as $3 \cdot 10^{-14}$ cm^2/s. This is in agreement with paper III where a value of $5 \cdot 10^{-14}$ cm^2/s is obtained for a similar device, but with a voltage of 1.5 V.

The unexpected decrease in reflectance with intercalation could be due to the initial absorption in c-WO_3 discussed in section 5.1.1 and shown in Fig. 5.4. The current density in Fig. 5.11 b) not reaching a maximum may indicate that the intercalation levels were lower than needed for the free-electron behaviour to occur. The total thickness of the layers in the ATF II device and the film for which the emittance was given in Fig. 5.4 were 1005 and 1450 nm respectively. The infrared reflectance in the ATF II device may therefore be dominated by interference effects.

The optical transmission spectra in the range 0.3 – 2.5 μm for the ATF III device are shown in Fig. 5.12. It is seen that the device exhibited a very low transmission in the NIR range in the coloured state, which could be used for greenhouse applications. In the intended application the NIR would be absorbed for water desalination, while the photosynthetically active radiation would be transmitted[67]. The ATF III device showed low reflectance modulation at these wavelengths (see paper V). Both spectra (coloured and bleached) had an average value of 0.2.

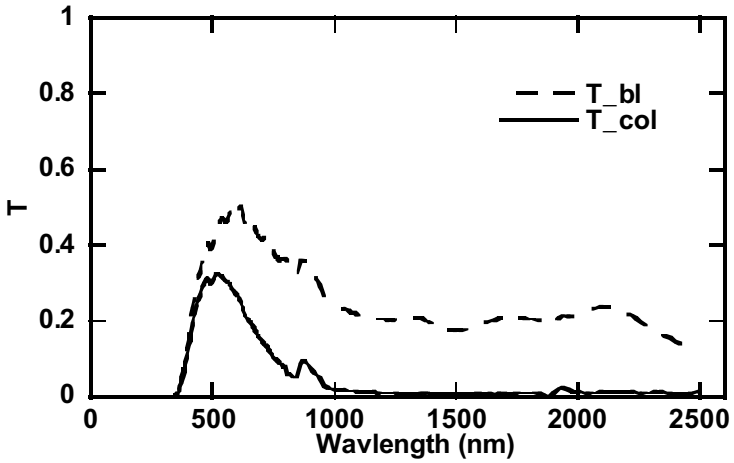

Fig. 5.12: Reflectance spectra in the range 0.3 – 2.5 μm, of an all-thin-film glass | ITO | $NiV_xO_yH_z$ | ZrO_2 | c-WO_3 | Al-grid | c-WO_3 device with two layers of c-WO_3 embedding the Al-grid. The spectra were taken when the c-WO_3 film was bleached and coloured. A voltage of –/+5 V was applied at the Al grid during intercalation/deintercalation.

It is interesting to note a difference in the visual appearance of the colouring of devices with a-WO_3 and c-WO_3. The (dark blue) colour of the devices with a-WO_3 starts around the edges of the Al-grid and diffuses out until the whole WO_3-area is coloured. The (light blue) colour of the c-WO_3 film starts homogeneously in the whole WO_3 area with the same intensity as around the grid. The dynamics of the processes do also differ, the a-WO_3 device colours much faster than the one with c-WO_3. The dense structure in c-WO_3 will inhibit the ions in their movement in the material, which could explain the slow colouring of the c-WO_3 device. These dynamic differences seem more pronounced in devices than in single films cycled in liquid electrolyte.

6 Summary

6.1 Summary and conclusions

This work has investigated the optical and thermal modulation of electrochromic thin film devices, and single thin films of a-WO_3 and c-WO_3. Single thin films were manufactured, and investigated in the wavelength range 0.3-50 μm. Laminated devices were manufactured, and investigated in the infrared range, 2-50 μm, for comparison. The all-thin-film (ATF) devices were manufactured, and investigated in the wavelength range 0.3-50 μm. The electrical properties of ATF devices were investigated.

The infrared optical properties of thin films of a-WO_3, c-WO_3 and nanocrystalline WO_3 were investigated for different amounts of intercalated Li ions. It was found that a-WO_3 showed as high modulation as c-WO_3 at infrared wavelengths, mainly due to interference effects. The emittance varied between 0.70 and 0.49 for the c-WO_3, between 0.52 and 0.72 for the a-WO_3 and between 0.59 and 0.76 for a nanocrystalline film. The interference effects made the reflectance of the c-WO_3 film decrease for low intercalation levels, while for $x \geq 0.05$ it exhibited a free-electron like behaviour and an increased reflectance. The nanocrystalline film exhibited a modulation similar to that of the a-WO_3 film, i.e., the reflectance decreased with intercalation level.

The optical properties of thin films of a-WO_3 and c-WO_3 were measured at wavelengths between 300 and 2500 nm, at different intercalation levels. The intercalating ions were Li. The absorption coefficient, obtained from measurement results on c-WO_3, was compared to large polaron theory. A good agreement between the peak position around 1.8 μm and the one predicted by theory, was found.

A laminated device based on a conventional design, where one of the ITO covered glass substrates was replaced with a Si/Al-grid substrate, was manufactured and optical spectra were obtained. The device exhibited a low emittance modulation, from 0.56 to 0.65. This design is not suitable for infrared radiation control.

All-thin-film devices, with $NiV_xO_yH_z$ as ion storage layer, a thin film of ZrO_2 as ion conductor and c-WO_3 and/or a-WO_3 as active layer were manufactured. The films were deposited onto ITO covered glass. The top

contact was an evaporated Al-grid. The devices were investigated by the isothermal transient ionic current (ITIC) technique, where a voltage is applied and the current is measured. It was found that the ZrO_2 layer probably is the rate limiting layer in this device. The proton diffusion coefficient was around 5×10^{-14} cm^2/s.

The optical properties of thin films of ATF devices were investigated and transmittance and reflectance spectra were recorded at wavelengths between 0.3 and 2.5 μm, for different intercalation levels. The visible transmittance, calculated from measurements, varied between 0.48 and 0.15 for the ATF device with a-WO_3, and between 0.46 and 0.29 for the ATF device with c-WO_3. The reflectance did not change much. The ATF device with c-WO_3, exhibited selective transmittance modulation. At near-infrared wavelengths the transmittance became almost zero, while in the visible range, it was around 0.3.

The infrared reflectance of ATF devices with different configurations was investigated in-situ at different intercalations levels. The emittance was calculated from the reflectance measurements. The emittance of the device with a-WO_3, varied between 0.33 and 0.59, while that for the device with c-WO_3 varied between 0.35 and 0.60 in the deintercalated and intercalated state respectively. This makes the ATF devices strong contenders to contemporary emittance modulating devices.

6.2 Suggestions for future work

6.2.1 Technical issues

Considering the devices for space applications, there are technical issues, that should be further investigated. The space organizations have standards for tests related to the space environment, such as radiation-, vacuum-, vibration-, thermal- and ougassing tests. Also durability tests in normal earth environment should be performed. The ATF devices in this work have been submitted to initial radiation tests[vii]. The film stack of the returned samples had partly detached from the substrate, but it is uncertain if this was due solely to the radiation.

Protons may not be the optimal ion to use; it could be very interesting to try Li. Initial efforts to intercalate Li into nickel oxide films have been performed within this work. The response was weak, and the limits for the reversible range seemed very well defined.

There is certainly a need for a protection layer in the space environment. Franke et. al[39] have reported on ZnSe as a candidate. Initial optical

[vii] The tests were performed at ESA Technical headquarter (ESTEC) in Holland.

measurements on CVD diamond films have been performed within this work. The diffuse transmittance was 0.5 at 10 μm for a film on a Si-substrate.

The ion conductor suffers quite often from short-circuits. This may originate from pin-holes, or particles that deposit the $NiV_xO_yH_z$ layer when the samples are stored outside the sputtering chamber. Samples have been prepared without having being extracted from the sputtering chamber, by the use of a shutter system covering the targets. There was no difference noticed in yield. Maybe a clean-room environment is needed to prevent dust and particles to deposit on the previous layer.

If the device is divided into individual sub-devices, the majority will still work if one of the sub-devices is destroyed by e.g. a micrometeorite. This is an ongoing project at ÅSTC[2], and it involves an advanced lithographic process to create independent contacts on the same substrate. Smaller devices will probably also increase the switching speed.

6.2.2 Scientific issues

The optical constants for all layers in a device should be determined to gain control of the interference effects and optimize the device performance. The inverse method[48] where fitting is done to the reflectance as a function of thickness, has been initially tested in this work. There is a problem to have good optical constants for the ITO.

The mixed conduction process in the ion conductor needs to be investigated to get control of the electron leakage current in the devices.

The reason for the slow kinetics in c-WO_3 is not understood, or why it colours more homogeneously than the a-WO_3, nor if these properties are connected.

6.2.3 Outlook

Recent trends indicate that both NASA (National Aeronaoutics and Space Administration) and ESA (European Space Agency) are interested in developing this type of thermal control for larger space craft such as communication satellites. This will increase the interest and research efforts within this field.

Summary of appended papers

Paper I

The low mass of a micro/nano spacecraft leads to low thermal inertia with rapid and large changes of temperature as a consequence. This calls for new solutions in thermal control such as a variable emittance panel. Such a device has been manufactured exhibiting a variable emittance between 0.56 and 0.65.

This work was an initial investigation of the infrared properties of a laminated device, where a Si/Al-grid acted as a semitransparent window during measurements. It was clear that the optical modulation was low, probably due to the polymer electrolyte and the Si substrate.

Paper II

Thin sputtered films of amorphous and crystalline tungsten trioxide were intercalated with Li ions in 1M $LiClO_4$ in propylene carbonate. The infrared reflectance was measured ex-situ at wavelengths between 2 and 50 μm for Li_xWO_3 of different thickness, d, and at different Li/W ratios, x.

This work was an initial optical investigation of intercalated thin films of sputtered a- and c-WO_3. The results on single layered films should indicate which type of film to use for devices and the amount of charge to intercalate. Initially c-WO_3 seemed to be most promising. However, it was found that interference effects in thick amorphous films gave rise to unpredicted high modulation at infrared wavelengths.

Paper III

An ATF device with WO_3 and NiO as active layers, and ZrO_2 as ion conductor has been studied using the Isothermal Transient Ionic Current (ITIC) technique. With the method applied it was found that the proton mobility for the whole device was characterized by a proton diffusion coefficient of the order of magnitude of 5×10^{-14} cm^2/s. The rate-limiting layer of the device is most likely the ZrO_2-electrolyte layer.

Paper IV

Thin films of polycrystalline tungsten trioxide were manufactured using dc magnetron sputtering. Li ions and electrons were intercalated into the sample that were submitted to optical characterization by spectrophotometry, in the visible and infrared ranges. The optical spectra were recorded at different

intercalation states, and the absorption of the films was obtained. At low intercalation levels, a pronounced absorption peak was observed centred at a wavelength of 1.8 μm. Upon intercalation, the inserted electrons enter the conduction band, but due to a strong electron-phonon interaction, they are believed to form localized polarons. Calculations of optical absorption by large polaron theory were carried out and the position of the observed peak was in good agreement with the theory.

Paper V

The optical properties of an all-thin-film electrochromic device, with a thin film of ZrO_2 acting as an ion conductor has been investigated. Transmission (T) and reflection (R) spectra were recorded in the wavelength range 300-2500 nm at different intercalation levels, both for single films and complete devices. The results show that T decreases significantly upon intercalation in the WO_3 thin films as well as in the devices. The reflectance only shows minor changes.

This work investigated the properties of the ATF in the visible spectral range. The intercalated c-WO_3 as a single film or in the ATF device exhibit a near-infrared transmission near zero, while the transmittance at visible wavelengths lies around 0.5.

Paper VI

Thin films of amorphous and polycrystalline tungsten oxide were produced by reactive dc magnetron sputtering, and nanocrystalline films were produced by advanced gas evaporation. The films were submitted to electrochemical intercalation of Li ions before infrared reflectance measurements were carried out.

This work investigated the infrared optical properties for a-WO_3, c-WO_3 and nanocrystalline WO_3. It was found that the emittance for the nanocrystalline film increased with intercalation. The emittance of the a-WO_3 film increased with intercalation and that of the c-WO_3 film decreased.

Paper VII

All-thin-film electrochromic devices for infrared emittance modulation were manufactured using dc magnetron sputtering. The devices were cycled electrochemically, and the optical signal was measured in-situ by spectrophotometry in the wavelength range 2 to 50 μm. The devices consisted of WO_3 as a main electrochromic layer, ZrO_2 as an ion conductor, and $NiV_xO_yH_z$ as a complementary electrochromic layer. The substrate was glass covered with indium tin oxide, and the front electrode was an evaporated Al grid. The highest emittance modulation was between $\varepsilon_{low}=0.33$ and $\varepsilon_{high}=0.59$, which compares favourably with previously studied variable emittance devices.

7 Elektrokroma tunnfilmskomponenter för optisk och termisk modulation

Denna avhandling handlar om ytor med styrbar emittans, d.v.s. förmågan att utstråla värme.

En avhandlings kortaste sammanfattning är ju titeln, så det verkar lämpligt att utgå från den då arbetet ska beskrivas.

7.1 Elektrokromism

Ett elektrokromt material kan ändra färg när man lägger en elektrisk spänning över det. Egenskapen elektrokromism är besläktad med den mer allmänt kända fotokromismen, som återfinns i glasögon som mörknar i solljuset. Hos elektrokroma material uppstår en liknande färgning då man tillför elektroner till materialet, och med omvänd polaritet kan materialet blekas igen.

En stor grupp av elektrokroma material är oxider av övergångsmetaller[4,5]. De är lämpliga att använda i applikationer då de kan tillverkas som tunna filmer, vars tjocklek är av storleksordningen några hundra nanometer (1 nm=10^{-9} m). Den vanligaste applikationen är ett s.k. ”smart fönster”[3] där persiennen ersätts med den elektrokroma filmen, som alltså kan göra fönstret mörkt (eller genomskinligt) vid behov. Förutom ”smarta fönster”[6] har även bilbackspeglar[7] och visir för motorcykelhjälmar[8] kommersialiserats.

Volframtrioxid, WO_3, är den i särklass mest undersökta elektrokroma övergångsmetalloxiden[4], och den uppvisar också den bästa modulationen. Elektrokroma egenskaper hos tunna filmer av WO_3 rapporterades för första gången 1969[25]. I detta arbete har tunna filmer av WO_3 använts som huvudsaklig (”aktiv”) del i komponenterna.

7.2 Elektrokroma tunnfilmskomponenter

En elektrokrom tunnfilmskomponent är uppbyggd som ett batteri, där joner flyttas fram och tillbaks genom en elektrolyt. När jonerna går in i t ex WO_3, drar de till sig elektroner (från en yttre krets), som reducerar W-jonen. Detta förändrar elektronernas högsta energinivå i materialet som börjar absorbera

infallande strålning, det blir alltså icke-transparent. I en elektrokrom tunnfilmskomponent behövs, utöver det elektrokroma materialet, elektriska ledare, en jonledare (elektrolyten) samt ett jonlager[viii]. I traditionella elektrokroma komponenter är elektrolyten en fast polymer, men i detta arbete har polymeren ersatts med en tunn film av zirkoniumdioxid, ZrO_2 (se avsnitt 7.3). Därför är den engelska titeln ”All-thin-film...”, för att betona att dessa tunnfilmskomponenter enbart består av tunna filmer.

7.3 Optisk och termisk modulation

”Optisk” avser i detta arbete strålning i våglängdsområdet 0.3 – 2.5 μm medan ”termisk” syftar på våglängdsområdet 2.5 – 50 μm. Elektrokroma tunnfilmskomponenter har sitt ursprung i det ”optiska” området, medan detta arbete även inkluderar det ”termiska” området, som är mindre utforskat. Det är inte självklart att ett material som modulerar i det ”optiska” intervallet, även gör det i det ”termiska”. Emittansen beräknas ur uppmätta data, och kan variera mellan 0 och 1.

Intresset för elektrokroma tunnfilmskomponenters termiska modulation är att de skulle kunna användas som temperaturkontroll på små satelliter. En satellits temperatur måste kontrolleras för att utrustningen ombord ska fungera. Satellittemperaturen ges till stor del av strålningsutbytet med omgivningen, och detta varierar när satelliten går in och ut ur jordskuggan. Strålningsutbytet (och således temperaturen) beror av satellitytans emittans, så det vore mycket fördelaktigt att kunna anpassa emittansen efter aktuell mängd infallande strålning. För små satelliter, som har ont om plats och är känsliga för temperatursvängingar (p g a den låga massan), är elektrokroma tunnfilmskomponenter därför mycket intressanta.

En konventionell elektrokrom komponent med polymer elektrolyt lämpar sig inte för rymdmiljön. Dels är det hög risk att polymeren förstörs i vakkumet, och dels bidrar den till att komponenten kommer utgöras av två substrat (t ex glasrutor) med polymeren emellan. Det extra substratet kommer hindra strålningen från det elektrokroma materialet (som måste ligga mot polymeren på insidan av glaset) att nå ut. Elektrokroma tunnfilmskomponenter för termisk modulation i detta arbete ser därför ut som i Figur 7.1. Substratet är glas täckt med indiumtennoxid (ITO) (som är en elektrisk ledare). På detta ligger $NiV_xO_yH_z$ som jonlager, ZrO_2 som jonledare, och WO_3 som det elektrokroma lagret. Överst deponeras en elektrisk ledare av Al i ett genombrutet mönster (”galler”) för att minska den

[viii] Jonlagret kan också vara ett elektrokromt material, men av en sådan typ så att det färgas då jonerna går ut ur filmen. På detta sätt förstärks effekten av den första filmen.

infraröda reflektansen som är karakteristisk för elektriskt ledande material. Jonerna som flyttas mellan filmerna utgörs här av protoner.

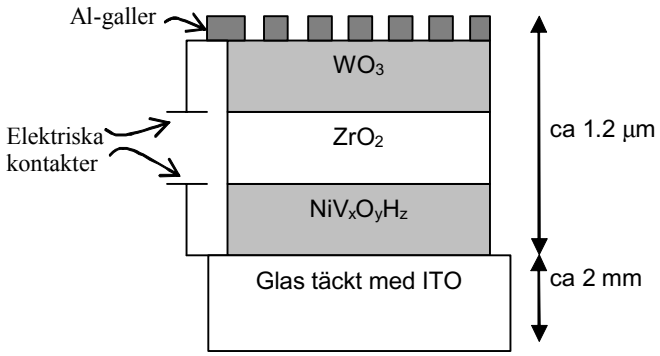

Figur 7.1: Genomskärning av en elektrokrom tunnfilmskomponent för optisk och termisk modulation. Substratet är glas med en ledande film av ITO. På detta ligger $NiV_xO_yH_z$ (jonlager), ZrO_2 (jonledare), WO_3, (aktiv film) och ett Al-galler som elektrisk kontakt överst. Genom att lägga på en spänning över kontakterna kan man få jonerna (protoner) att vandra mellan filmen av $NiV_xO_yH_z$ och den av WO_3. Notera de olika längdskalorna.

7.4 Resultat av arbetet

I arbetet har ingått att tillverka och analysera tunna filmer av olika typer av WO_3, och olika typer av hela tunnfilmskomponenter.

Mätningarna av de tunna filmerna gav att olika typer av WO_3 (amorf och kristallin film) uppvisade ungefär lika hög emittansmodulation. Detta berodde förmodligen på att modulationen till största delen uppkom genom interferenseffekter i filmerna och inte genom materialens inneboende egenskaper (som borde gett ett högre värde för den kristallina filmen).

I en mer fundamental undersökninng av WO_3 fann man god överensstämmelse mellan experimentella data och polaronteori[50], som kan förklara ledningsegenskaper hos WO_3, och vad som händer när materialet absorberar strålning.

En konventionell elektrokrom komponent med polymer-elektrolyt tillverkades och analyserades. Den uppvisade låg emittansmodulation (0.56-0.65).

De elektrokroma tunnfilmskomponenterna undersöktes elektriskt, och man fann att den långsammaste rörlelsen förmodligen skedde i ZrO_2-filmen.

Komponenterna visade sig ha god emittansmodulation, mellan 0.33 och 0.59, vilket står sig väl gentemot andra emittansmodulerande komponenter.

Acknowledgements

This work was carried out at the Division for Solid State Physics and at the Ångström Space Technology Centre, Department of Materials Science, Uppsala University. I have also been part of the graduate school Advanced Micro Engineering. I would like to acknowledge Lars Stenmark and Claes-Göran Granqvist for financial support, thank you both for the possibility to be a part of your research groups.

I would then like to acknowledge Gunnar, Thank you! for sharing of your outstanding knowledge in physics (which is fruitfully combined with a remarkable memory), but even more for being so very supportive, helpful and humorous in all the windings throughout this work.…Lars, Thank you for sharing of your experience from thirty years in space business and for your never-ending optimism and laughter down the corridor. ...Johan, Thank you for your ability to catch the essence, clarify, and make the next step obvious. ... Andris, Thank you for having lots of time, patience and answers. ... Shuxi, Thank you for fixing the equipment in a professional way.

I thank all of you who who have contributed to make my stay at Ångström enjoyable at SSP, ÅSTC and otherwise, I wish you all the best! Especially I'm greatful for the interesting discussions with C-G, Barbara, Richard, Annika, Martin, Andreas, Arne, Mari-Louise, Herman, Lars B, Örjan, Solveig, Jacob, Torbjörn, Arne, Ewa, Maria S, Kristina, Anders, Jesper, Maria B, Ulrika, Ylvi, Lotta, Lars K, Anders E, Tobias, Kerstin, Jonas M, Annette, Lisen, Monica and Monika, and probably many more...

I would also like to take the opportunity to acknowlege my colleague and friend AnnaKarin, Thank you for precious friendship and support, interesting discussions and all the wonderful laughters! … my friend Anna, Thank you for all the good times (and Signalanalyslab)! … my friends Suzi and Charlotte, Thank you for always make me feel welcome at the west coast! … my mother and father, Irene and Lars, Thank you for always being there! … my cousins Ulf and Lalita, Thank you for your life long friendships!

And finally, for sharing all the linseed oil colour and candlelights, and all the amazing love, I thank you my dear Magnus!

Uppsala, december 2003
Anna-Lena Larsson

References

1. Wertz J.R. and Larson W.J., (Eds.), Space mission analysis and design, Kluwer Academic Publishers, Dordrecht, 1999.

2. http://www.astc.material.uu.se

3. Svensson J.S.E.M. and Granqvist C.G., Electrochromic coatings for "smart windows", *Proc. SPIE* **502**, 30-37 (1985).

4. Granqvist C.G., Handbook of inorganic electrochromic materials, Elsevier, Amsterdam, 1995.

5. Monk P.M.S., Mortimer R.J. and Rosseinsky D.R., Electrochromism : Fundamentals and applications, VCH, Weinheim, 1995.

6. http://www.flabeg.de

7. http://www.gentex.com/corp_npd.html

8. http://www.chromogenics.se/index_eng.htm

9. Zhang J.-G., Benson D.K., Tracy C.E., Deb S.K., Czanderna A.W. and Crandall R.S., Optimization study of solid-state electrochromic devices based on WO/sub 3//lithium-polymer electrolyte/V/sub 2/O/sub 5/ structures, *J. Electrochem. Soc.* **141**, 2795-2800 (1994).

10. Azens A., Isidorsson J., Karmhag R. and Granqvist C.G., Highly transparent Ni-Mg and Ni-V-Mg oxide films for electrochromic applications, *Thin Solid Films* **422**, 1-3 (2002).

11. Ahn K.-S., Nah Y.-C., Park J.-Y., Sung Y.-E., Cho K.-Y., Shin S.-S. and Park J.-K., Bleached state transmittance in charge-unbalanced all-solid-state electrochromic devices, *Appl. Phys. Lett.* **82**, 3379-3381 (2003).

12. Goldner R.B., Arntz F.O., Dickson K., Goldner M.A., Haas T.E., Liu T.Y., Slaven S., Wei G., Wong K.K. and Zerigian P., Some lessons learned from

research on a thin film electrochromic window, *Solid State Ionics* **70/71**, 613-618 (1994).

13. Cogan S.F., Rauh R.D., Klein J.D., Nguyen N.M., Jones R.B. and Plante T.D., Variable transmittance coatings using electrochromic lithium chromate and amorphous WO/sub 3/ thin films, *J. Electrochem. Soc.* **144**, 956-960 (1997).

14. Mathew J.G.H., Sapers S.P., Cumbo M.J., O'Brien N.A., Sargent R.B., Raksha V.P., Lahaderne R.B. and Hichwa B.P., Large area electrochromics for architectural applications, *J. Non-Cryst. Solids* **218**, 342-346 (1997).

15. O'Brien N.A., Gordon J., Mathew H. and Hichwa B.P., Electrochromic coatings-applications and manufacturing issues, *Thin Solid Films* **345**, 312-318 (1999).

16. Granqvist C.G. and Hultåker A., Transparent and conducting ITO films: New developments and applications, *Thin Solid Films* **411**, 1-5 (2002).

17. Azens A., Kullman L. and Granqvist C.G., Ozone coloration of Ni and Cr oxide films, *Solar Energy Mater. Solar Cells* **76**, 147-153 (2003).

18. Granqvist C.G., Electrochromic tungsten oxide films: review of progress 1993-1998, *Solar Energy Mater. Solar Cells* **60**, 201-262 (2000).

19. Hutchins M.G., Butt N.S., Topping A.J., Gallego J., Milne P., Jeffrey D. and Brotherston I., Tantalum oxide thin film ionic conductors for monolithic electrochromic devices, *Proc. SPIE* **4458**, 120-127 (2001).

20. Armitage R., Rubin M., Richardson T., O'Brien N. and Chen Y., Solid-state gadolinium-magnesium hydride optical switch, *Appl. Phys. Lett.* **75**, 1863-1865 (1999).

21. Mercier V.M.M. and van der Sluis P., Toward solid-state switchable mirrors using a zirconium oxide proton conductor, *Solid State Ionics* **145**, 17-24 (2001).

22. Hutchins M.G., Butt N., Topping A., Gallego J., Milne P., Jeffrey D. and Brotherston I., Infrared reflectance modulation in tungsten oxide based electrochromic devices, *Electrochim. Acta* **46**, 1983-1988 (2001).

23. Franke E.B., Trimble C.L., Hale J.S., Schubert M. and Woollam J.A., Infrared switching electrochromic devices based on tungsten oxide, *J. Appl. Phys.* **88**, 5777-5784 (2000).

24. www.ne.se

25. Deb S.K., Novel electrographic system, *Appl. Optics* **3**, 192-195 (1969).

26. Zhong Q., Dahn J.R. and Colbow K., Lithium intercalation into WO_3 and the phase diagram of Li_xWO_3, *Phys. Rev. B* **46**, 2554-2560 (1992).

27. Strømme Mattsson M., Cation intercalation in sputter-deposited W oxide films, *Phys. Rev. B* **58**, 11015-11022 (1998).

28. Hansen M., Constitution of binary alloys, MacGraw-Hill, New York, 1958.

29. Powell R.J. and Spicer W.E., Optical properties of NiO and CoO, *Phys. Rev. B* **2**, 2182-2193 (1970).

30. Avendaño E., Electrochromic properties of nickel based oxide films, Licentiate thesis, (Department of Materials Science, Uppsala University, 2002).

31. Preusser S., Stimming U. and Wipperman K., An optical and electrochemical investigation of ZrO_2 thin films (from nm to mm thickness), *Electrochim. Acta* **39**, 1273-1280 (1994).

32. Jonsson A.K., Charge transport in transition metal oxide thin films and electrochromic devices, Ph.D. Thesis, (Dep. of Materials Science, Uppsala University, 2002).

33. http://www.appliedfilms.com

34. Such K., Stevens J.R., Wieczorek W., Siekierski M. and Florjanczyk Z., Polymer solid electrolytes from the PEG-PMMA-$LiCF_3SO_3$ system, *J. Polym. Sci. Pt. B* **32**, 2221-2233 (1994).

35. Butt N.S., Electrochromic devices for solar and thermal radiation controls, Ph.D. Thesis, (Solar Energy Materials Research Laboratory, Oxford Brookes University, 1999).

36. Chandrasekhar P., Electrochromic display device, World Patent WO9944093 (1999).

37. Chandrasekhar P., Zay B.J., Birur G.C., Rawal S., Pierson E.A., Kauder L. and Swanson T., Large, switchable electrochromism in the visible through far-infrared in conducting polymer devices, *Adv. Funct. Mater.* **12**, 95-103 (2002).

38. Bessière A., Beluze L., Morcrette M., Viana B., Badot J.C. and Lucas V., Electrochromic variation of the infrared emissivity in tungsten oxide compounds, *Radiation Effects & Defects in Solids* **158**, 215-220 (2003).

39. Franke E., Neumann H., Schubert M., Trimble C.L., Yan L. and Woollam J.A., Low-orbit-environment protective coating for all-solid-state electrochromic surface heat radiation control devices, *Surf. Coat. Technol.* **151-152**, 285-288 (2002).

40. Bessière A., Marcel C., Morcrette M., Tarascon J.-M., Lucas V., Viana B. and Baffier N., Flexible electrochromic reflectance device based on tungsten oxide for infrared emissivity control, *J. Appl. Phys.* **91**, 1589-1594 (2002).

41. Osiander R., Champion J., Darrin M., Douglas D., Swanson T., Allen J. and Wykoff E.E., in: Proc. NanoTech 2002, **2002-5766**, 2002.

42. Douglas D.M., Swanson T., Osiander R., Champion J., Darrin A.G., Biter W. and Chandrasekhar P., Development of the variable emittance thermal suite for the space technology 5 satellite, NASA Center for AeroSpace Information (CASI), Tech. rep. **20020039293**, 2001

43. Grob L. and Swanson T.D., Parametric study of variable emissivity radiator surfaces, NASA Center for AeroSpace Information (CASI), Tech. rep. **20000021239**, 2000

44. International standard, ISO/CIE 10526, CIE standard Colorimetric Illuminants (1999).

45. Born M. and Wolf E., Principles of optics, Pergamon Press, London, 1980.

46. Azzam R.M.A. and Bashara N.M., Ellipsometry and Polarized Light, Oxford : North-Holland, Amsterdam, 1977.

47. Hong W.Q., Extraction of extinction coefficient of weak absorbing thin films from special absorption, *J. Phys. D: Appl. Phys.* **22**, 1384-1385 (1989).

48. Singleton E.B. and Shirkey C.T., Optical constants in the IR from thin film interference and reflectance: the reststrahlen region of muscovite mica, *Appl. Optics* **22**, 185-189 (1983).

49. Landau L., On the motion of electrons in a crystal lattice, *Sov. Phys. JETP* **3**, 664-665 (1933).

50. Calvani P., Optical properties of polarons, *Riv. Nuovo Cimento* **24**, 1-71 (2001).

51. Klingshirn C.F., Semiconductor optics, Springer, Berlin, 1997.

52. Berggren L., Azens A. and Niklasson G.A., Polaron absorption in amorphous tungsten oxide films, *J. Appl. Phys.* **90**, 1860-1863 (2001).

53. Private communication, Sernelius B.E.

54. Sarafin T.P., Spacecraft structures and mechanisms, Microcosm Press, Calofornia, and Kluwer Academic publishers, Dordrecht, 1995.

55. Gilmore D.G., Satellite thermal control handbook, The aerospace corporation, 1994.

56. Lugenkov V. and Barabash S., The main principles of thermal calculations for space instruments., Swedish Institute of Space Physics, Tech. rep. **042**, 1993

57. Tachikawa S. and Ohnishi A., Development of a variable emittance radiator based on a perovskite manganese oxide, *Journal of thermophysics and heat transfer* **17**, 264-268 (2003).

58. Klintberg L., Karlsson M., Stenmark L., Schweitz J.-A. and Thornell G., A large stroke, high force paraffin phase transition actuator, *Sensors and Actuators A (Physical)* **A96**, 189-195 (2002).

59. Veszelei M., Preparation and characterization of sputtered metal oxides and nitrides for optical applications., Ph.D. Thesis, (Dep. of Materials Science, Uppsala University, 1997).

60. Heavens O.S., Optical properties of thin solid films, Dover, New York, 1991.

61. Vossen J.L. and Kern W., Thin film processes, Academic Press, Boston, 1991.

62. Brundle C.R., Evans J.C.A. and Wilson S., (Eds.), Encyclopedica of Materials Characterization, (Butterworth-Heinemann Manning, Boston, 1992).

63. Cullity B.D., Elements of x-ray diffraction, Addison-Wesley, Massachusetts, 1956.

64. National Bureau of Standards, Standard Reference Materials Lg no 2019(a) and 2021.

65. Solis J.L., Hoel A., Lantto V. and Granqvist C.G., Infrared spectroscopy study of electrochromic nanocrystalline tungsten oxide films made by reactive advanced gas deposition, *J. Appl. Phys.* **89**, 2727-2732 (2001).

66. Frenning G., Jonsson A.K., Larsson A.L. and Strømme M., Theoretical investigation of ion conduction in three-layered ion-conductor systems: derivation of the isothermal transient ionic current and frequency-dependent impedance, *J. Appl. Phys.* **94**, 1629-1638 (2003).

67. Chaibi M.T., System design operation and performance of roof-integrated desalination in greenhouses, Solar Energy, (*submitted).*

Acta Universitatis Upsaliensis

Comprehensive Summaries of Uppsala Dissertations from the Faculty of Science and Technology

Editor: The Dean of the Faculty of Science and Technology

A doctoral dissertation from the Faculty of Science and Technology, Uppsala University, is usually a summary of a number of papers. A few copies of the complete dissertation are kept at major Swedish research libraries, while the summary alone is distributed internationally through the series *Comprehensive Summaries of Uppsala Dissertations from the Faculty of Science and Technology*. (Prior to October, 1993, the series was published under the title "Comprehensive Summaries of Uppsala Dissertations from the Faculty of Science".)

Distribution:
Uppsala University Library
Box 510, SE-751 20 Uppsala, Sweden
www.uu.se, acta@ub.uu.se

ISSN 1104-232X
ISBN 91-554-5844-0